ADVANCED MATERIALS
www.advmat.de

Antigen Presenting Cell Mimetic Lipid Nanoparticles for Rapid mRNA CAR T Cell Cancer Immunotherapy

*Ann E. Metzloff, Marshall S. Padilla, Ningqiang Gong, Margaret M. Billingsley, Xuexiang Han, Maria Merolle, David Mai, Christian G. Figueroa-Espada, Ajay S. Thatte, Rebecca M. Haley, Alvin J. Mukalel, Alex G. Hamilton, Mohamad-Gabriel Alameh, Drew Weissman, Neil C. Sheppard, Carl H. June, and Michael J. Mitchell**

Chimeric antigen receptor (CAR) T cell therapy has achieved remarkable clinical success in the treatment of hematological malignancies. However, producing these bespoke cancer-killing cells is a complicated ex vivo process involving leukapheresis, artificial T cell activation, and CAR construct introduction. The activation step requires the engagement of CD3/TCR and CD28 and is vital for T cell transfection and differentiation. Though antigen-presenting cells (APCs) facilitate activation in vivo, ex vivo activation relies on antibodies against CD3 and CD28 conjugated to magnetic beads. While effective, this artificial activation adds to the complexity of CAR T cell production as the beads must be removed prior to clinical implementation. To overcome this challenge, this work develops activating lipid nanoparticles (aLNPs) that mimic APCs to combine the activation of magnetic beads and the transfection capabilities of LNPs. It is shown that aLNPs enable one-step activation and transfection of primary human T cells with the resulting mRNA CAR T cells reducing tumor burden in a murine xenograft model, validating aLNPs as a promising platform for the rapid production of mRNA CAR T cells.

1. Introduction

The first chimeric antigen receptor (CAR) T cell therapy was approved by the US Food and Drug Administration (FDA) in 2017 for the treatment of relapsed or refractory acute lymphoblastic leukemia.[1] Since then, five additional CAR T cell therapies have been approved for the treatment of hematological malignancies.[2–6] This success has spurred the development of CAR T cell therapies for the treatment of solid tumors and non-malignant diseases.[7–12] Currently, the FDA-approved CAR T cells are autologous, meaning that they are produced from a patient's own T cells that have been engineered to express the CAR construct.[13] This synthetic receptor fuses a monoclonal antibody against a disease target with intracellular stimulatory and costimulatory domains to achieve both

A. E. Metzloff, M. S. Padilla, N. Gong, M. M. Billingsley, X. Han, D. Mai, C. G. Figueroa-Espada, A. S. Thatte, R. M. Haley, A. J. Mukalel, A. G. Hamilton, M. J. Mitchell
Department of Bioengineering
School of Engineering and Applied Science
University of Pennsylvania
Philadelphia, PA 19104, USA
E-mail: mjmitch@seas.upenn.edu

M. Merolle
Department of Pathobiology
School of Veterinary Medicine
University of Pennsylvania
Philadelphia, PA 19104, USA

D. Mai, N. C. Sheppard, C. H. June, M. J. Mitchell
Abramson Cancer Center
Perelman School of Medicine
University of Pennsylvania
Philadelphia, PA 19104, USA

The ORCID identification number(s) for the author(s) of this article can be found under https://doi.org/10.1002/adma.202313226

DOI: 10.1002/adma.202313226

D. Mai, N. C. Sheppard, C. H. June, M. J. Mitchell
Center for Cellular Immunotherapies
Perelman School of Medicine
University of Pennsylvania
Philadelphia, PA 19104, USA

M.-G. Alameh, D. Weissman
Department of Medicine
University of Pennsylvania
Philadelphia, PA 19104, USA

M.-G. Alameh, D. Weissman, M. J. Mitchell
Penn Institute for RNA Innovation
Perelman School of Medicine
University of Pennsylvania
Philadelphia, PA 19104, USA

N. C. Sheppard, C. H. June
Department of Pathology and Laboratory Medicine
Perelman School of Medicine
University of Pennsylvania
Philadelphia, PA 19104, USA

M. J. Mitchell
Institute for Immunology
Perelman School of Medicine
University of Pennsylvania
Philadelphia, PA 19104, USA

specificity and potency in cancer cell killing, respectively.[13] To produce CAR T cells, a patient's T cells are harvested via leukapheresis. The isolated T cells are activated, viral vectors are employed to incorporate genetic constructs encoding for CAR into the genomes of the T cells, and the CAR T cells are expanded in bioreactors before reinfusion into patients.[13]

Although CAR T cells produced in this way can bring about durable cancer remission, two serious side effects–cytokine release syndrome and neurotoxicity–are common.[14–16] These toxicities generally occur within days of CAR T cell administration and can be treated with interleukin-6 receptor monoclonal antibodies and corticosteroids.[17,18] Additionally, CAR T cells also persist in the body for years, exerting their targeting effects long after a patient's cancer has been cleared.[19] In the context of CAR T cells for hematological malignancies, this leads to B cell aplasia and hypogammaglobulinemia.[14,20] These adverse effects have led to the exploration of alternative, non-viral methods of CAR T cell engineering, such as the delivery of CAR-encoding messenger RNA (mRNA) to T cells.[21–31] mRNA does not integrate into the genome, so it results in only transient CAR expression, which may aid in preventing the long-term side effects of CAR T cell therapy.[21,28–31] Additionally, non-viral delivery methods could reduce manufacturing costs, increase cargo capacity, and increase safety.[32] Therefore, mRNA CAR T cell therapy is being explored for the treatment of a variety of cancers.[21,24,29–31]

In preclinical studies, mRNA CAR T therapy has been found to be as effective as viral CAR T therapy at lowering short-term cancer burden with less inherent toxicity,[21,24] which has resulted in the initiation of several clinical trials.[28,33-36,79] In these clinical trials, CAR mRNA was delivered to patients' isolated T cells ex vivo by electroporation, a method where electric pulses are used to generate transient pores in the cell membrane.[37] However, electroporation requires specialized equipment and results in high rates of cell death as well as altered gene expression in the surviving cell population.[37,38] An alternative approach is to encapsulate CAR mRNA in lipid or polymer nanoparticles.[24-26] Nanoparticles do not require specialized equipment for cellular delivery and can be engineered to stabilize their mRNA cargo, enhance intracellular delivery, and reduce cytotoxicity compared to electroporation.[25,26,39,40] Ionizable lipid nanoparticles (LNPs) are one of the most clinically advanced nanoparticle platforms.[39,41,42] Their successful use as the carrier for the COVID-19 mRNA vaccines validated their potency and safety in hundreds of millions of patients around the world.[43] Additionally, they can be rapidly produced at large scales. Recent studies have explored using nanoparticles to produce mRNA CAR T cells directly in the body.[12,24] While such in situ CAR T cell engineering has great potential, there are several drawbacks that have not yet been overcome, such as off-target CAR delivery and infusion reactions upon systemic administration of nanoparticles, hindering the advancement of in situ CAR T cell therapy into the clinic. Ex vivo CAR T cell therapy is still the current clinical gold standard.

Aware of this potential, we previously optimized an LNP platform for ex vivo CAR mRNA delivery to primary human T cells and demonstrated its superiority over electroporation.[25,26] Still, in order to express LNP-delivered mRNA, T cells must be activated.[25,26,28] In the body, T cells are activated when they interact with antigen-presenting cells (APCs). A primary activation signal is provided when major histocompatibility complex proteins, displaying antigens, on an APC interact with CD3/T cell receptor (TCR) protein complexes on a T cell. However, for full activation of a T cell, a costimulatory activation signal must also be provided. This occurs when CD80 or CD86 proteins on the APC interact with CD28 proteins on the T cell (**Figure 1a**).[44] To engineer T cells ex vivo, this process is mimicked with antibodies against CD3 and CD28, which are often attached to either magnetic beads for easy removal or to APC-mimicking platforms.[45–52] In a traditional LNP administration workflow, the activating beads are added to T cells in culture. After waiting 24 h for activation, the beads are removed with a magnet, and then mRNA LNPs are added (Figure 1b, top).[25,26] Though this strategy is effective, it increases the time and complexity of the workflow while decreasing cell yields during bead extraction. Thus, this work aimed to eliminate the need for beads in the mRNA CAR T cell engineering workflow, so that mRNA CAR T cells could be produced in a single, rapid step.

We hypothesized that directly conjugating CD3 and CD28 antibody fragments to the surface of our LNPs could bypass the need for pretreatment with activating beads to engineer mRNA CAR T cells. In this study, we used a thiol-maleimide reaction to conjugate CD3 and CD28 antibody fragments to the surface of our previously optimized T cell LNPs. We call these activating LNPs (aLNPs) as they mimic the activating function of APCs (Figure 1b, bottom). We first show that aLNPs efficiently transfect primary human T cells with mRNA in the absence of activating beads before optimizing the ratio of CD3 to CD28 antibody fragments conjugated to the aLNP surface. We then demonstrate that anti-CD19 CAR T cells generated with aLNPs perform potent cancer cell killing ex vivo, readily proliferate, and express cell-surface activation markers at levels comparable to those of bead-activated T cells. Finally, we demonstrate that the adoptive transfer of anti-CD19 CAR T cells generated with aLNPs reduces tumor burden in a xenograft murine model of leukemia, validating aLNPs as a platform to efficiently produce a functional mRNA CAR T cell therapy.

2. Results

2.1. Formulation and Characterization of aLNPs

The T cell LNPs we previously developed are composed of four traditional components: an ionizable lipid which is neutrally charged at physiological pH but positively charged in acidic pH to aid in endosomal escape, a helper phospholipid to promote LNP structure and organization, cholesterol to provide LNP stability, and lipid-anchored polyethylene glycol (PEG) to encourage LNP

M. J. Mitchell
Cardiovascular Institute
Perelman School of Medicine
University of Pennsylvania
Philadelphia, PA 19104, USA
M. J. Mitchell
Institute for Regenerative Medicine
Perelman School of Medicine
University of Pennsylvania
Philadelphia, PA 19104, USA

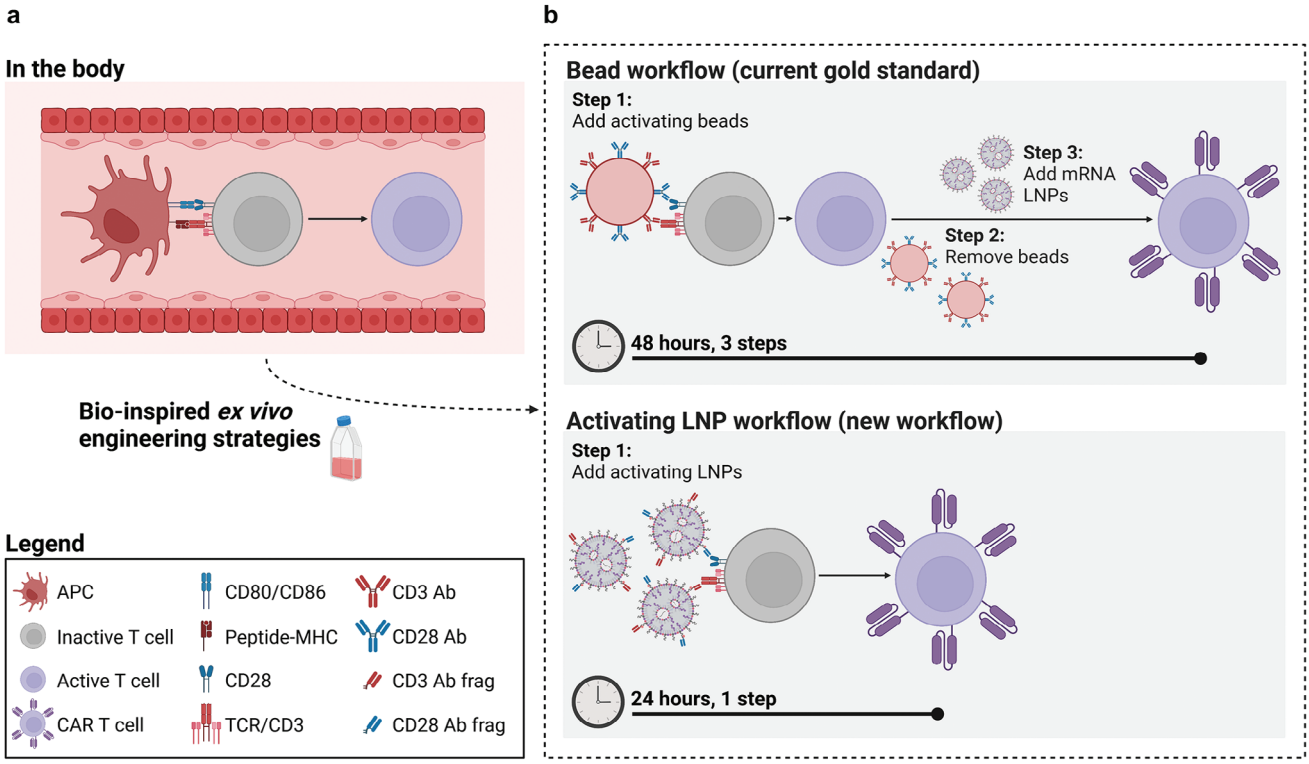

Figure 1. Antigen presenting cell mimetic activating lipid nanoparticles (aLNPs) rapidly activate primary human T cells and transfect them with CAR mRNA in a single step. a) In the body, T cells are activated when they engage with antigen presenting cells (APCs). For complete activation, APCs must provide T cells with a primary and a costimulatory signal. The primary signal occurs when APC peptide-MHC interacts with T cell CD3/TCR. The costimulatory signal occurs when APC CD80/CD86 interacts with T cell CD28. Once activated, the T cell can carry out its effector function in the body. b) Top: To engineer chimeric antigen receptor (CAR) T cells outside of the body with lipid nanoparticles (LNPs), T cells must first be activated. Antibodies against CD3 and CD28, often conjugated to magnetic beads, are used to mimic APC activation before dosing the T cells with mRNA LNPs. Bottom: Activating LNPs (aLNPs) are developed by conjugating CD3 and CD28 antibody fragments to the surface of the LNPs. aLNPs combine the activating properties of the beads and the mRNA-delivering capabilities of traditional LNPs, enabling activation of and CAR mRNA delivery to T cells in a single, rapid step. (a,b) were created with BioRender.com.

self-assembly and reduce LNP aggregation.[41,53] It has been previously shown that the inclusion of maleimide functional groups on the LNP surface enables the binding of antibody fragments that have had their disulfide bonds reduced to thiol groups.[54–56] We chose to use this conjugation strategy here due to its simplicity, efficiency, and cost-effectiveness. Because it relies on endogenous disulfide bonds that are present in all antibodies, no additional coupling molecules are required. Furthermore, we wanted to enzymatically remove Fc regions to prevent possible negative inflammatory side effects if, in the future, the aLNP platform were to be systemically administered for the in situ engineering of cells. This strategy works with antibodies that have had their Fc regions removed.

Therefore, for this study, our previously optimized LNPs were formulated with a fraction of the lipid-anchored PEG replaced by lipid-anchored PEG-maleimide to form maleimide-LNPs (mal-LNPs) (**Figure 2a**). An S_N2 reaction was employed to synthesize the ionizable lipid C14-4 by reacting a polyamine core with an excess of 1,2-epoxytetradecane (Figure 2b). Then, C14-4 was combined with the helper phospholipid dioleoylphosphatidylethanolamine (DOPE), cholesterol, lipid-anchored PEG (14:0 PEG2000 PE), lipid-anchored PEG-maleimide (DSPE-PEG2000 Maleimide), and mRNA in a microfluidic mixing device to form mal-LNPs. Separately, human CD3 and CD28 antibodies were enzymatically cleaved with IdeZ into $F(ab')_2$ and Fc fragments, and then treated with dithiothreitol (DTT) to reduce the disulfide bonds on the $F(ab')_2$ fragments to thiol groups, producing a mixture of Fd', LC, and F(ab') fragments (Figure S1, Supporting Information). The cleaved and reduced CD3 and CD28 antibody fragments were added to the mal-LNPs for surface conjugation via a thiol-maleimide reaction to produce aLNPs. Following conjugation, aLNPs were purified by size exclusion chromatography to remove the unbound Fc fragments as well as any unbound Fd', LC, or F(ab') fragments (Figure 2c).

Dynamic light scattering was used to characterize mal-LNPs before and after antibody fragment conjugation (Figure 2d). The hydrodynamic diameter, measured as intensity-weighted Z-average, showed an increase in particle size from 115.5 nm for mal-LNPs to 189.7 nm for aLNPs. We interpreted the increase in size between the two particles as confirmation that antibody fragments were successfully bound to the aLNP surface. We also observed that the LNPs maintained their polydispersity after antibody conjugation with a polydispersity index (PDI) of 0.259 for mal-LNPs and 0.263 for aLNPs, which suggests that the size exclusion chromatography was effective at isolating the antibody-bound particles. Therefore, we concluded that the

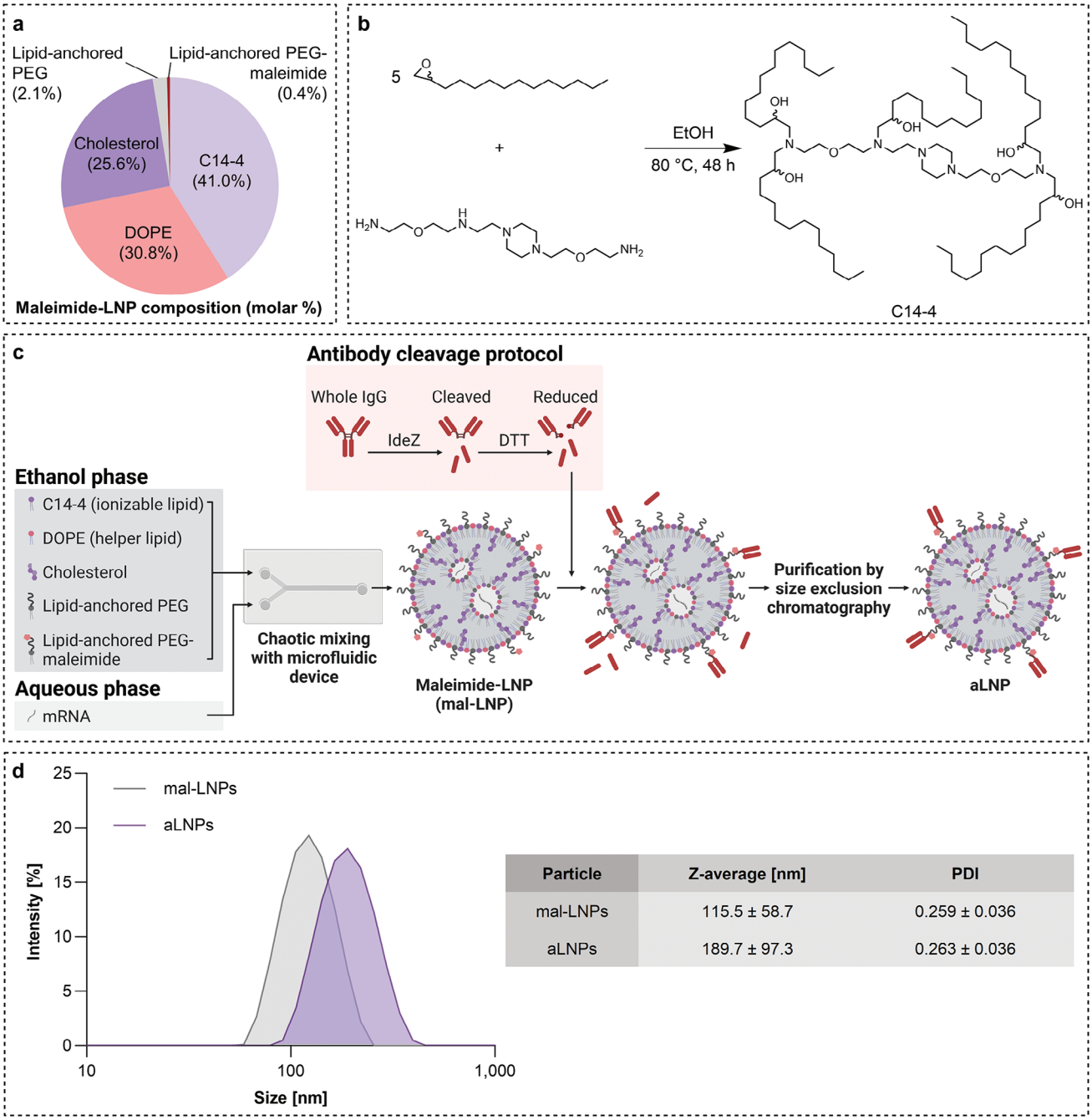

Particle	Z-average [nm]	PDI
mal-LNPs	115.5 ± 58.7	0.259 ± 0.036
aLNPs	189.7 ± 97.3	0.263 ± 0.036

Figure 2. Formulation and characterization of activating LNPs (aLNPs). a) Molar composition of maleimide-LNPs (mal-LNPs). PEG, polyethylene glycol. DOPE, dioleoylphosphatidylethanolamine. C14-4, an ionizable lipid. b) S_N2 synthesis of the ionizable lipid C14-4 from 1,2-epoxytetradecane (top left) and a polyamine core (bottom left). c) The formulation of maleimide-LNPs (mal-LNPs) by microfluidic mixing, the cleavage and reduction of antibody fragments, and the conjugation of antibody fragments onto the mal-LNP surface to generate aLNPs. d) Left, the hydrodynamic diameter (intensity weighted Z-average) distributions of mal-LNPs and 1:1 anti-CD3:anti-CD28 aLNPs. Right, Z-average and polydispersity index (PDI) measurements, collected in triplicate. Reported values are average Z-average ± the calculated SD (calculated SD = $\sqrt{\text{average PDI} \times (\text{averageZ-average})^2}$) and average PDI ± SD of the three PDI measurements. (c) was created with BioRender.com.

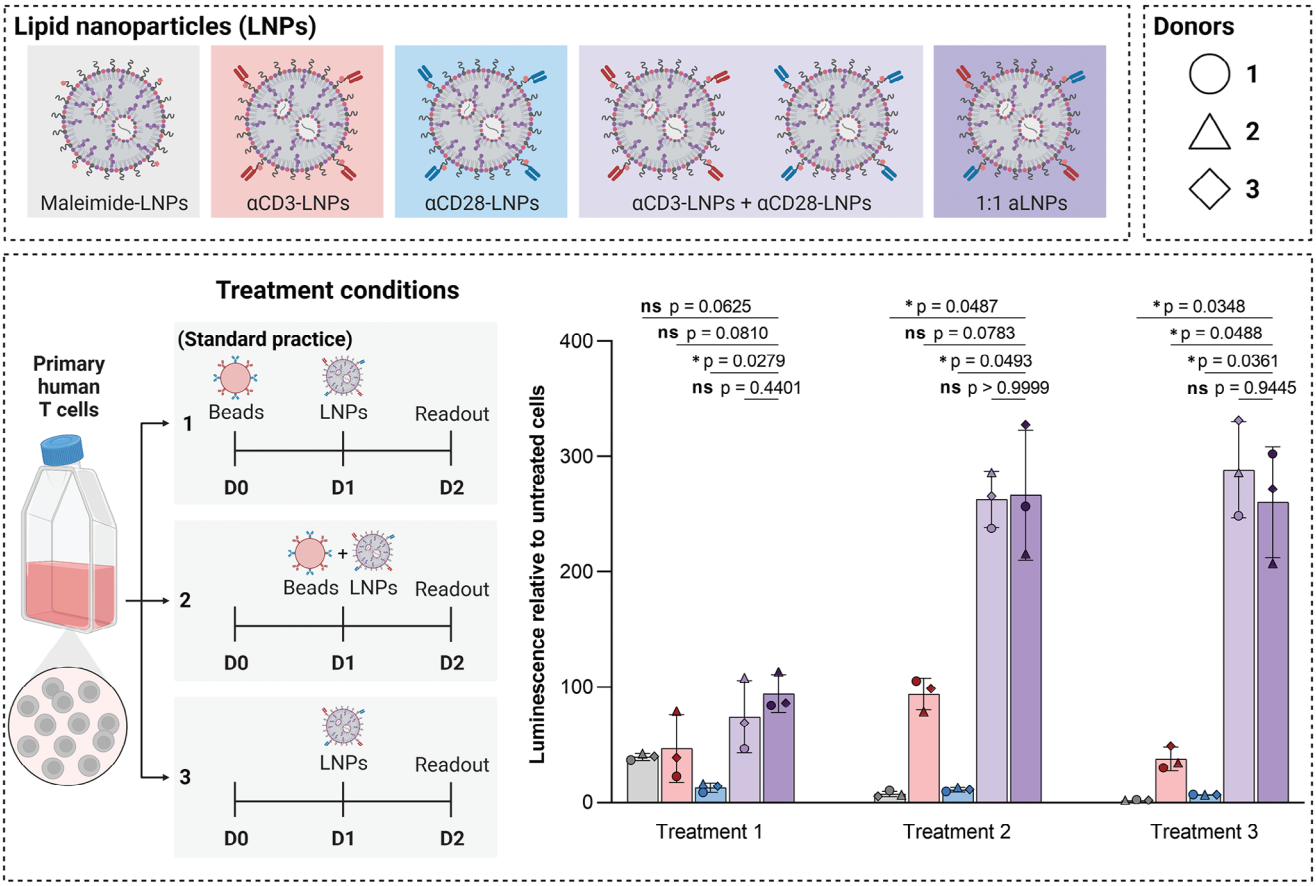

Figure 3. aLNPs efficiently transfect primary human T cells with luciferase mRNA in the absence of activating beads. Luminescence in primary human T cells dosed with one of five mRNA lipid nanoparticles (LNPs) and exposed to one of three treatment conditions. Each bar represents the mean data collected for three different donors that are normalized to untreated cells within each donor. On every bar, the mean normalized luminescence for each donor is plotted as a shape (circle, triangle, or rhombus) to highlight donor-to-donor variability. Differences in LNP means within each treatment were assessed with a two-way repeated measures ANOVA with post-hoc *t*-tests using Tukey's correction for multiple comparisons. Only results of comparisons to aLNPs are shown. $n = 3$ donors, with $n = 3$ replicates per donor. Data are presented as mean ± SD. $^*p \leq 0.05$, ns = not significant. Created with BioRender.com.

maleimide-thiol conjugation strategy can be successfully applied to our T cell LNPs to produce aLNPs.

2.1.1. aLNPs Efficiently Transfect Primary Human T Cells without Activating Beads Ex Vivo

We next devised an ex vivo screen that would allow us to 1) test the ability of aLNPs to deliver their mRNA cargo to primary human T cells in the presence and absence of activating beads, and 2) explore the individual effects of conjugated CD3 and CD28 antibody fragments on LNP-mediated mRNA delivery. For this screen, LNPs were formulated to encapsulate mRNA encoding for the established model cargo luciferase, an enzyme that produces luminescence proportional to its concentration upon the addition of the luciferin substrate.[57,58]

For the initial screen, five LNP groups were explored: i) mal-LNPs, ii) mal-LNPs conjugated to CD3 antibody fragments (αCD3-LNPs), iii) mal-LNPs conjugated to CD28 antibody fragments (αCD28-LNPs), iv) an equal-part mixture of αCD3-LNPs and αCD28-LNPs, and v) mal-LNPs conjugated with a 1:1 ratio of CD3:CD28 antibody fragments (aLNPs). Each group was added to primary human T cells according to one of three different treatment schemes that were performed in parallel on cells from the same donor (**Figure 3**, and Tables S1 and S2, Supporting Information). For treatment 1, activating beads were added to the cells on the day the cells were received from the donor (day 0) and LNPs were added 24 h later (day 1). For treatment 2, activating beads and LNPs were both added on day 1. For treatment 3, LNPs were added on day 1 and activating beads were not added. In all three treatments, luciferin was added to the cells and luminescence was assessed on day 2, 24 h after dosing with LNPs. The full screen was completed on primary human T cells from three different donors.

The results of the screen highlight that aLNPs alone are a promising alternative to the traditional activating bead and transfection agent workflow (Figure 3). Compared to the standard workflow of mal-LNPs in treatment 1, we observed that aLNPs and αCD3-LNPs + αCD28-LNPs administered in treatment 3 resulted in 6.6-fold and 7.3-fold increases in luminescence,

respectively, while the mal-LNPs, αCD3-LNPs, and αCD28-LNPs in treatment 3 resulted in decreased luminescence. This indicates that only aLNPs or αCD3-LNPs + αCD28-LNPs can potently transfect primary human T cells with mRNA in the absence of activating beads, while LNPs without antibody fragments or with only CD3 or only CD28 antibody fragments cannot–highlighting the importance of providing T cells with both primary and costimulatory activation signals. Secondly, we noted that there were no statistically significant differences in luminescence between the aLNP group and the αCD3-LNP + αCD28-LNP group in any of the treatment conditions, suggesting that it does not matter whether CD3 and CD28 antibody fragments are on the same or separate LNPs as both strategies are similarly effective at facilitating LNP uptake and mRNA translation. Surprisingly, we also noted that the aLNP groups for treatments 2 and 3 both had 2.8-fold higher luminescence than the aLNP group for treatment 1. We hypothesize that pre-treatment with activating beads sterically inhibits aLNP uptake resulting in lower luminescence. Finally, we observed that aLNPs perform just as well in treatment 3 as they do in treatment 2, indicating that activating beads are neither required for nor do they enhance mRNA delivery by aLNPs, thus validating aLNPs as a stand-alone T cell transfection reagent. Due to the simplicity of a single-LNP system, we decided to move forward with aLNPs as they provide a one-step method to transfect primary human T cells without the need for activating beads. Furthermore, if added to T cells on day 0 with a readout on day 1, aLNPs enable the full engineering workflow to be completed in 24 h rather than 48 h.

2.1.2. aLNP CD3 to CD28 Antibody Fragment Ratio Optimization Enhances CAR mRNA delivery Ex Vivo, and the Resulting CAR T Cells Effectively Kill Leukemia Cells Ex Vivo

After confirming that aLNPs were able to transfect primary human T cells with mRNA in the absence of activating beads, we evaluated whether adjusting the ratio of CD3:CD28 antibody fragments on the aLNP surface would impact transfection. We performed this screen first with mRNA encoding the model cargoes EGFP and mCherry, and second with mRNA encoding a second-generation human CD19-targeted CAR. Interestingly, we observed different trends for EGFP and mCherry (Figures S2–S4, Supporting Information) compared to CAR, which we hypothesize may be due to the inert nature of the fluorescent reporter proteins compared to the biological activity of the CAR. Understanding the full effect of mRNA transcript on aLNP-mediated mRNA delivery is a topic of interest and something that we plan to explore in future studies. However, because CAR mRNA is our desired aLNP cargo, herein we used the findings from the CAR screen to inform our aLNP optimization. CD19-targeted CAR mRNA was synthesized via in vitro transcription with uridine residues fully replaced by N1-methyl-pseudouridine (m1ψ) residues to improve translation and decrease immune recognition.[59] This mRNA was formulated into aLNPs with 50:1, 10:1, 1:1, 1:10, and 1:50 ratios of CD3:CD28 antibody fragments on their surfaces which were administered to primary human T cells (**Figure** 4a,b).

We first observed that all aLNP variants resulted in substantial CAR positivity 24 h after aLNP administration, ranging from 33.5% CAR+ for 50:1 aLNPs to 84.1% CAR+ for 1:50 aLNPs, highlighting the benefit of conjugating CD3 and CD28 antibody fragments to the LNP surfaces, regardless of ratio. Furthermore, we noted a clear increase in transfection efficiency with a higher proportion of CD28 antibody fragments, as 50:1, 10:1, 1:1, 1:10, and 1:50 aLNPs resulted, respectively, in 33.5%, 39.3%, 62.9%, 82.7%, and 84.1% CAR positivity. The mean fluorescence intensities (MFIs) of the cell populations also exhibited the same upward trend; we observed the lowest MFI of 1620 for 50:1 aLNPs and the highest MFI of 14600 for 1:50 aLNPs–a 9-fold increase. When compared to 1:1 aLNPs, 50:1 and 10:1 aLNPs resulted in significantly lower CAR positivity and MFIs, whereas 1:10 and 1:50 aLNPs resulted in significantly higher CAR positivity and MFIs. Therefore, we concluded that aLNPs with greater numbers of CD28 than CD3 antibody fragments more effectively transfect primary human T cells with CD19-directed CAR mRNA.

Next, we performed a tumor cell co-culture experiment to assess whether there would be differences in the cytotoxic ability of CAR T cells generated with the various aLNPs (Figure 4c,d). Twenty-four hours after aLNP administration, CAR T cells produced with 50:1, 10:1, 1:1, 1:10, and 1:50 aLNPs encapsulating CAR mRNA were mixed with luciferase-expressing Nalm6 CD19+ human acute lymphoblastic leukemia cells in various CAR T cell to Nalm6 cell ratios. After 48 h, the percentage of Nalm6 cells killed was quantified. Robust, dose-dependent killing was observed for all aLNP-generated CAR T cells, with 67.6–90.9% killing at the highest CAR T cell to Nalm6 cell ratio, and 24.9–33.9% killing at the lowest CAR T cell to Nalm6 cell ratio (Figure 4e). Thus, we concluded that all aLNP variants can be used to produce therapeutically efficacious CAR T cells. However, we did note that for the three highest CAR T to Nalm6 cell ratios, the 50:1 and 10:1 aLNPs resulted in significantly elevated killing compared to 1:1 aLNPs, whereas no significant differences were found when 1:10 and 1:50 aLNPs were compared to 1:1 aLNPs. We then investigated whether any of the aLNPs were toxic when administered to primary human T cells by adding a reagent that produces luminescence proportional to the amount of ATP, and therefore to the number of viable, metabolically active cells (Figure S5, Supporting Information). Minor toxicity was observed for 10:1, and 50:1 aLNPs, with viabilities of 97.6%, and 90.2%, respectively. However, no toxicity was observed for 1:50, 1:10, or 1:1 aLNPs.

In all, these ex vivo results informed the selection of an optimal aLNP for continued investigation. An ideal aLNP platform would demonstrate a high MFI as previous studies have found that low CAR expression limits the efficacy of CAR T cells in vivo.[60] It would also be essential that the chosen aLNP demonstrate a high transfection efficiency to maximize CAR T cells produced from the limited resource of isolated patient T cells. Further, the aLNPs would not be toxic to the T cells, and the resulting CAR T cells would be highly effective at killing tumor cells. With these parameters in mind, we chose to move forward with our 1:10 aLNPs, as we hypothesized that they would provide the best balance of the factors above. Once deciding to move forward with 1:10 aLNPs, we characterized them using two additional methods (Tables S3 and S4, Supporting Information). First, we measured mRNA encapsulation efficiency of 83.0% for 1:10 aLNPs.[25,61,62] Although still high, 83.0% is slightly lower than the 94.3% encapsulation

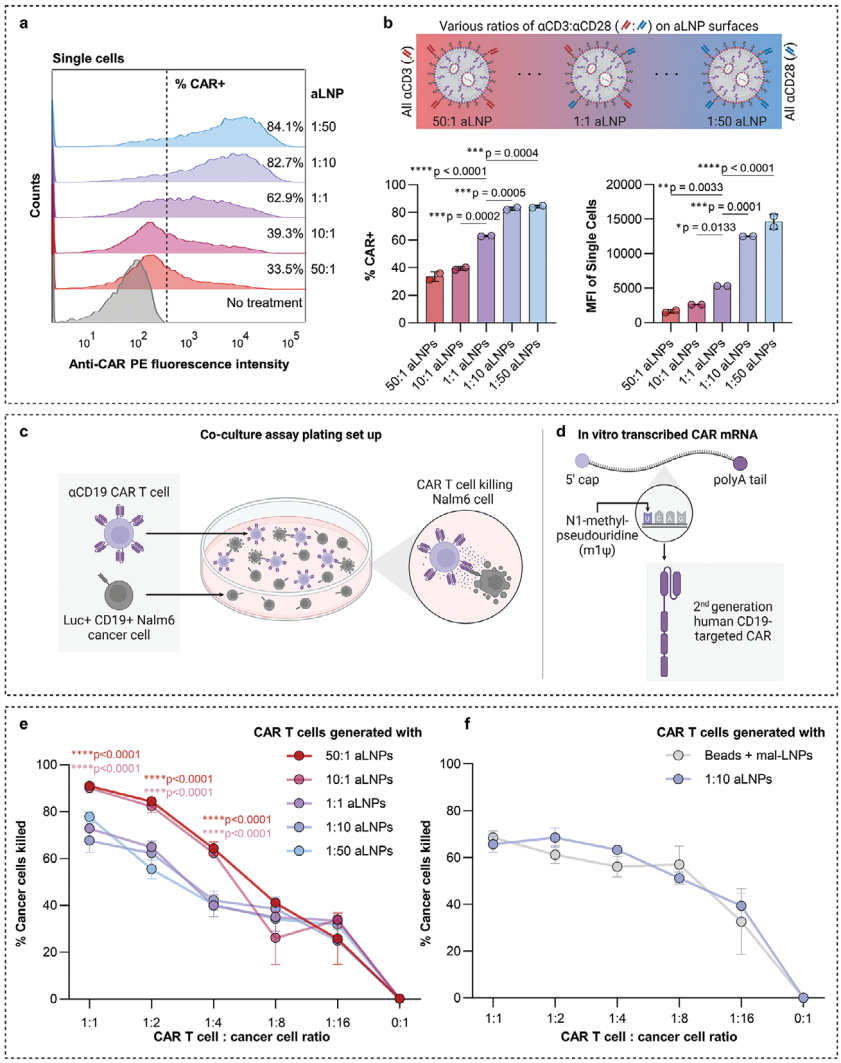

Figure 4. The ratio of CD3 to CD28 antibody fragments on the aLNP surface influences the number and mean fluorescence intensity (MFI) of CAR transfected cells, which effectively kill leukemia cells ex vivo. a) Representative flow cytometry histograms obtained from primary human T cells treated with CD19-directed CAR mRNA aLNPs containing varying ratios of CD3:CD28 antibody fragments on their surfaces. CAR+ cells are defined as those to the right of the dashed line. b) Top: Schematic depicting the various aLNP treatments. Bottom, left: Percentage of single cells that are CAR+ after each aLNP treatment, from the same experiment as the representative histograms. Bottom, right: MFI of single cells after each aLNP treatment, from the same experiment as the representative histograms. $n = 1$ donor, with $n = 2$ replicates. For each bar graph, differences between group means were assessed by an ordinary one-way ANOVA with post-hoc *t*-tests using Tukey's correction for multiple comparisons. Only comparisons to 1:1 aLNPs are shown. c) Co-culture assay plating setup. d) In vitro transcribed CD19-targeted CAR mRNA. e) Percentage of Nalm6 cancer cells killed when cultured with CAR T cells generated with aLNPs containing 50:1, 10:1, 1:1, 1:10, and 1:50 ratios of CD3:CD28 antibody fragments on their surfaces. $n = 1$ donor, with $n = 3$ replicates per donor, from the same experiment as (a) and (b). Differences in treatment mean within each CAR T cell:cancer cell ratio were assessed by a two-way ANOVA with post-hoc *t*-tests using Tukey's correction for multiple comparisons. Only significant comparisons to 1:1 aLNPs are shown. f) Percentage of Nalm6 cancer cells killed when cultured with CAR T cells generated with beads + mal-LNPs or 1:10 aLNPs. $n = 3$ donors, with $n = 3$ replicates per donor. Assay results for a single donor are shown, with results for additional donors included in Figure S6, Supporting Information. Differences in treatment means within each CAR T cell:cancer cell ratio were assessed by a two-way ANOVA with post-hoc *t*-tests using Šídák's correction for multiple comparisons. Not shown = not significant. For (a,b,e,f) data are presented as mean ± SD. $*p \leq 0.05$, $**p \leq 0.01$, $***p \leq 0.001$, $****p \leq 0.0001$. (b–d) were created with BioRender.com.

efficiency measured for mal-LNPs, which suggests possible rupturing of some aLNPs due to shear stress during size exclusion chromatography. Second, we measured CD3 and CD28 antibody fragment concentrations of 12.7 and 109 ng μL^{-1}, respectively, in a 1:10 aLNP preparation, confirming that the 1:10 ratio in which the antibody fragments are added to the LNP mixture is maintained upon conjugation. Furthermore, when these concentrations are converted to molarities, they indicate that essentially all mal-PEG molecules are antibody-bound.

As an additional experiment, 1:10 aLNPs encapsulating CAR mRNA were administered to primary human T cells with a control of beads + mal-LNPs. The resulting CAR T cells were mixed with Nalm6 leukemia cells and, as before, we observed

robust, dose-dependent Nalm6 killing. Both 1:10 aLNP and bead + mal-LNP generated CAR T cells resulted in ≈70% killing at the highest CAR T cell to Nalm6 cell ratio and ≈35% killing at the lowest CAR T cell to Nalm6 cell ratio. Within each of the co-culture ratios, no statistically significant difference was found between CAR T cells generated with beads + mal-LNPs and CAR T cells generated with 1:10 aLNPs (Figure 4f). The co-culture experiment was repeated using primary human T cells from two additional donors and similar results were obtained (Figure S6, Supporting Information). Therefore, we concluded that CAR T cells produced by 1:10 aLNPs and beads + mal-LNPs are equivalently effective, validating bead-free mRNA CAR T cell production using 1:10 aLNPs. Finally, we treated primary human T cells with escalating doses of 1:10 aLNPs and assessed CAR positivity and viability 24 h after aLNP administration (Figures S7 and S8, Supporting Information). We observed a plateau in CAR positivity between 400 and 600 ng mRNA per 60 000 T cells and thus used a 400 ng dose for all subsequent studies.

2.2. Anti-CD19 CAR T Cells Generated with aLNPs Readily Proliferate, Maintain Cytotoxicity following Expansion, and have an Activated Phenotype

In the clinic, activating beads are used not only to activate T cells but also to expand their population. Therefore, we investigated whether 1:10 aLNPs and activating beads differ in their capacity to mediate T cell expansion. Prior to treatment with beads + mal-LNPs or 1:10 aLNPs, primary human T cells were stained with a fluorescent dye that binds to cellular amines. Each time the bead- or aLNP-stimulated cells underwent cellular division, the dye was diluted–thus distinct proliferative generations appeared as leftward-shifted peaks on flow cytometry histograms (**Figure 5a**). Bead- or aLNP-stimulated cultures were analyzed on days 2, 4, and 6 post-treatment. On day 4, beads had driven slightly more proliferation than aLNPs, with most of the bead-stimulated cells being third or fourth-generation cells, whereas the aLNP-stimulated cells were spread across parental, second-, third-, and fourth-generations. However, by day 6, the aLNPs had mediated substantially more proliferation than the beads, with most aLNP-stimulated cells spread over the fifth, sixth, and seventh generations, while most bead-stimulated cells were only fourth or fifth generation. Therefore, we concluded that 1:10 aLNPs elicit robust T cell proliferation.

To assess the therapeutic efficacy of these aLNP-expanded CAR T cells, we set up another Nalm6 co-culture killing assay, this time using primary human T cells that had been treated with 1:10 aLNPs 4 days previously, as compared to 1 day previously in Figure 4. Before setting up the assay, flow cytometry indicated that 59.8% of the T cells were CAR positive, indicating substantial residual CAR expression 4 days after aLNP addition (Figure 5b). These CAR T cells were plated in co-culture with Nalm6 leukemia cells and Nalm6 killing was quantified 48 h later (Figure 5c). As before, potent, dose-dependent Nalm6 cell killing was observed with 96.1% killing at the highest CAR T to Nalm6 cell ratio and 37.9% killing at the lowest. Therefore, we concluded that aLNP-expanded CAR T cells maintain their cytotoxicity for at least 4 days post aLNP administration.

Next, to better understand the aLNP-generated cell product, we used flow cytometry to characterize the expression of CCR7 and CD45RA on the surface of primary human T cells 3 days following treatment with either beads + mal-LNPs or 1:10 aLNPs (Figure 5d,e). Compared to the bead-generated cell product, the aLNP cell product retains a higher level of CCR7 expression, indicating retention of the less differentiated central memory (CM) phenotype which is preferable for an infusion product.[63] Furthermore, the bead-generated cell product has a higher population of CD45RA-positive terminally differentiated TEMRA cells, which is undesirable in an infusion product.[63] Thus, we concluded that 1:10 aLNPs can produce a cell infusion product with a desirable phenotype.

We also explored whether CAR T cells produced by beads + mal-LNPs versus 1:10 aLNPs differ in their activation states or in their secretion of effector cytokines prior to exposure to target cells. To assess activation status, we quantified CD25, CD69, and CD44 expression on the surface of primary human T cells 24 h after receiving no treatment (NT), LNPs with only CD3 antibody fragments on their surface (αCD3), LNPs with only CD28 antibody fragments on their surface (αCD28), beads + mal-LNPs (B+L), or 1:10 aLNPs (1:10) (Figure 5f, and Figures S9 and S10, Supporting Information). Beads + mal-LNPs and aLNPs resulted in significant upregulation of CD25, CD69, and CD44 compared to no treatment, indicating T cell activation.[64,65] Overall, we concluded that beads and 1:10 aLNPs are similarly potent activators of primary human T cells. Additionally, we observed that, in general, αCD3-LNPs caused intermediate effects over no treatment and αCD28-LNPs produced minor effects over no treatment, which highlights the need to provide T cells with both primary and costimulatory activation signals, whether on beads or on aLNPs.

We also quantified the concentrations of granzyme B, perforin, and soluble FasL–effector cytokines used for T cell-mediated killing–as well as tumor necrosis factor-alpha (TNFα) and interferon-gamma (IFNγ)–pro-inflammatory cytokines secreted by activated T cells–in the media of primary human T cells that received no treatment, αCD3-LNPs, αCD28-LNPs, beads + mal-LNPs, or 1:10 aLNPs (Figure S11, Supporting Information). Interestingly, we observed differences in the concentrations of effector cytokines for cells treated with beads + mal-LNPs compared to cells treated with aLNPs. Cells treated with beads + mal-LNPs produced higher levels of granzyme B, whereas cells treated with aLNPs produced higher levels of perforin and soluble FasL. We also observed that the cells treated with beads + mal-LNPs expressed significantly more TNFα and IFNγ than the cells treated with 1:10 aLNPs but, since the two types of CAR T cells performed equivalent cancer cell killing, this difference may not be critical to therapeutic efficacy.

Additionally, we performed two experiments to investigate the mechanism of aLNP uptake. In the first experiment, primary human T cells were pre-treated with various inhibitors of cellular uptake pathways prior to dosing with beads + mal-LNPs or 1:10 aLNPs (Figure S12, Supporting Information). For both groups, pre-treatment with amiloride, an inhibitor of macropinocytosis, resulted in the lowest expression of cargo mRNA, indicating that macropinocytosis is a predominant mechanism of both mal-LNP and aLNP uptake. Macropinocytosis is substantially upregulated in activated T cells, so this finding is consistent with

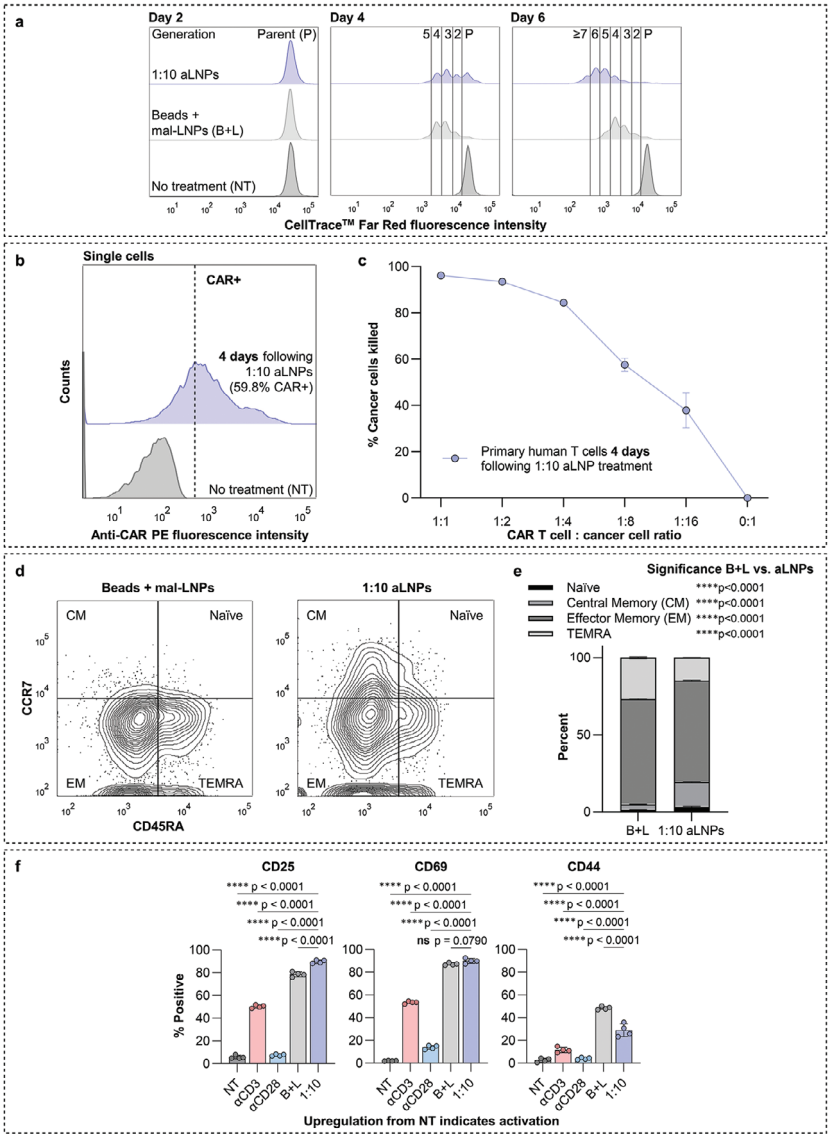

Figure 5. Anti-CD19 CAR T cells generated with aLNPs readily proliferate, maintain cytotoxicity following expansion, and have an activated phenotype. a) Flow cytometry histograms of primary human T cells stained with CellTrace Far Red at 2, 4, and 6 days post-treatment with beads + mal-LNPs (B+L) or 1:10 aLNPs (1:10). Each proliferative generation appears as a distinct leftward-shifted peak in the flow cytometry histogram. $n = 1$ donor, with $n = 2$ replicates. b) Representative flow cytometry histograms obtained from primary human T cells 4 days after the cells received no treatment (NT) or 1:10 aLNPs. CAR+ cells are defined as those to the right of the dashed line. c) Percentage of Nalm6 cancer cells killed after 48 h when cultured with the 4-day-post-aLNP CAR T cells shown in (b). $n = 1$ donor, with $n = 3$ replicates per donor. d) Representative flow cytometry plots showing CCR7 versus CD45RA expression for primary human T cells 3 days following treatment with beads + mal-LNPs (B+L) or 1:10 aLNPs. $n = 1$ donor, with $n = 3$ replicates per donor. e) Quantification of Naïve, central memory (CM), effector memory (EM), and TEMRA population sizes for the cells treated in (d). Differences in population sizes between B+L and 1:10 aLNPs were assessed by a two-way ANOVA with post-hoc *t*-tests using Šídák's correction for multiple comparisons. f) Percentages of primary human T cells expressing CD25, CD69, and CD44, as assessed via flow cytometry, 24 h after receiving no treatment (NT), LNPs with only CD3 antibody fragments on their surface (αCD3), LNPs with only CD28 antibody fragments on their surface (αCD28), beads + mal-LNPs (B+L), or 1:10 aLNPs (1:10). $n = 1$ donor, with $n = 4$ replicates. For each graph, differences between all group means were assessed by an ordinary one-way ANOVA with post-hoc *t*-tests using Tukey's correction for multiple comparisons. Only results of comparisons to 1:10 aLNPs are shown. For (b,c,e,f) data are presented as mean ± SD. $^*p \leq 0.05$, $^{**}p \leq 0.01$, $^{***}p \leq 0.001$, $^{****}p \leq 0.0001$, ns = not significant.

expectation.[66,67] In the second experiment, primary human T cells were pre-treated with CD3 and CD28 antibody Fabs to block the binding of beads or aLNPs to CD3/CD28 on the T cell surface, preventing activation (Figure S13, Supporting Information). Fabs were used rather than full divalent antibodies to preclude T cell activation due to antibody-mediated receptor crosslinking. After blocking, cells were treated with beads + DiR-labeled mal-LNPs or aLNPs. For both beads + mal-LNPs and aLNPs, it was found that Fab blocking only slightly reduced LNP uptake, indicating that LNPs can still enter blocked cells. Interestingly, however, Fab blocking drastically decreased cargo EGFP mRNA expression in the bead + mal-LNP group whereas it did not decrease

EGFP expression in the aLNP group. New evidence suggests that internalized TCR complexes can signal from the endosome,[68] and it is known that activated T cells have increased levels of translation.[69] Therefore, the elevated EGFP mRNA expression in blocked cells treated with aLNPs indicates that aLNPs may be able to facilitate activation signaling from the endosome. This could be an advantage of having the activation signal coupled to the aLNP, as opposed to separately on the bead.

2.3. Adoptive Transfer of Anti-CD19 CAR T Cells Generated with aLNPs Reduces Tumor Burden In Vivo

We then tested the efficacy of 1:10 aLNP-generated CAR T cells in a murine xenograft model of leukemia. Due to its transience, mRNA CAR T cell therapy is indicated in cases where tumor burden is low. Therefore, we employed a mouse model that mimics low leukemic burden. We inoculated NOD.Cg-Prkdc^{scid}Il2rg^{tm1Wjl}/SzJ (NSG) immunodeficient mice with luciferase-expressing CD19+ Nalm6 cells. Four days later, 2×10^6 anti-CD19 CAR T cells generated with aLNPs, untransfected T cells, or PBS were administered to each mouse. To counteract the transience of mRNA expression, the treatments were re-administered 3 and 6 days following the initial administration (**Figure 6**a, and Figures S14 and S15, Supporting Information).

Periodically throughout the treatment, mice were imaged for bioluminescence corresponding to tumor burden and the average total flux per mouse was recorded at each imaging time point. From day 2 onward, mice treated with aLNP-generated CAR T cells had the lowest tumor burden of the three groups. From day 5 onward, mice treated with aLNP-generated CAR T cells had significantly lower tumor burden than mice treated with PBS, and, from day 6 and onward, mice treated with untransfected T cells and mice treated with PBS had no significant difference in tumor burden. On day 14, the final day of the experiment, the luminescent signal corresponding to tumor burden in mice treated with aLNP-generated CAR T cells was 2.09-fold lower than in mice that received PBS, and 1.84-fold lower than in mice that received untransfected T cells (Figure 6b,c). It was also observed that treatment with aLNP-generated CAR T cells extended survival by 6 days compared to treatment with PBS or untransfected T cells, a statistically significant improvement, and administration of untransfected T cells did not significantly extend survival compared to PBS (Figure 6d). Therefore, we conclude that CAR T cells generated with 1:10 aLNPs effectively reduce tumor burden and extend survival in a mouse model of leukemia.

We then set up a second experiment to compare the efficacy of repeated administration of 1:10 aLNP CAR T cells to a single administration of lentiviral CAR T cells expressing the same anti-CD19 CAR (Figure S16, Supporting Information). Because lentiviral CAR T cells permanently express CARs whereas aLNP mRNA CAR T cells transiently express CARs, we carefully considered what dose of lentiviral CAR T cells to administer. Since mRNA expression wanes, the initial number of 2×10^6 mRNA CAR T cells decreases with time post-administration, whereas the number of lentiviral CAR T cells will stay the same or increase due to CAR T cell expansion upon antigen recognition.[70] Therefore, we decided to inject mice with a single dose of 1×10^6 lentiviral CAR T cells.

Throughout the treatment, mice were imaged and the average total flux per mouse corresponding to tumor burden was recorded. On days 2, 3, and 6, mice treated with lentiviral CAR T cells had the lowest average tumor burden. However, by day 9, the lowest average tumor burden was observed in mice treated with aLNP CAR T cells, and this trend was maintained throughout the remainder of the study (Figure 6e,f). On day 17, the final day that all study mice were alive, mice treated with aLNP CAR T cells and mice treated with lentiviral CAR T cells had tumor burdens that were both significantly lower than mice treated with PBS and not significantly different from each other. We also noted that treatment with lentiviral CAR T cells extended survival over PBS by 8 days, and treatment with 1:10 aLNP CAR T cells extended survival over PBS by 17 days, both significant extensions in survival (Figure 6g), thus solidifying the therapeutic potential of repeated administration of CAR T cells generated with 1:10 aLNPs.

3. Discussion

Using mRNA LNPs to produce transient yet potent CAR T cells ex vivo is an active area of investigation. However, T cells must be activated in order to express LNP-delivered mRNA. In the body, T cells are activated when they engage with APCs. For complete activation, T cells must receive primary and costimulatory signals via APC engagement with the T cell surface molecules CD3/TCR and CD28, respectively. To engineer CAR T cells ex vivo, this process is mimicked with antibodies against CD3 and CD28 often conjugated to magnetic beads or to other APC mimicking platforms. While effective, this increases the complexity of CAR T cell production because the beads must be removed prior to clinical administration. We hypothesized that directly conjugating CD3 and CD28 antibody fragments to the LNP surface could eliminate the need for activating beads in the mRNA CAR T cell engineering process, enabling rapid, one-step production of mRNA CAR T cells.

Thus, in this work, we developed aLNPs–T cell activating lipid nanoparticles with surface-conjugated human CD3 and CD28 antibody fragments (Figure 2). We demonstrated that aLNPs efficiently transfect primary human T cells with luciferase mRNA in the absence of activating beads (Figure 3). We optimized the ratio of CD3 to CD28 antibody fragments on the aLNP surface for CD19-directed CAR mRNA delivery and demonstrated that the resulting aLNP-generated CAR T cells perform potent cancer cell killing ex vivo (Figure 4). We then demonstrated that anti-CD19 CAR T cells generated with aLNPs readily proliferate, maintain cytotoxicity following expansion, and have an activated phenotype (Figure 5). Finally, we determined that the adoptive transfer of anti-CD19 CAR T cells generated with aLNPs reduces tumor burden in a xenograft mouse model of leukemia, validating aLNPs as a platform to produce functional mRNA CAR T cell therapy (Figure 6). aLNPs have the potential to shorten the complex mRNA CAR T cell engineering process. By eliminating the time required for pre-activation, aLNPs reduce the cell culture time required to generate mRNA CAR T cells by a factor of 2, from 48 to 24 h, which could help mRNA CAR T therapies to reach patients faster. Furthermore, the reduction in cell culture time–as well as the elimination of the need for activating beads–could result in considerable decreases in mRNA CAR T cell manufacturing costs.

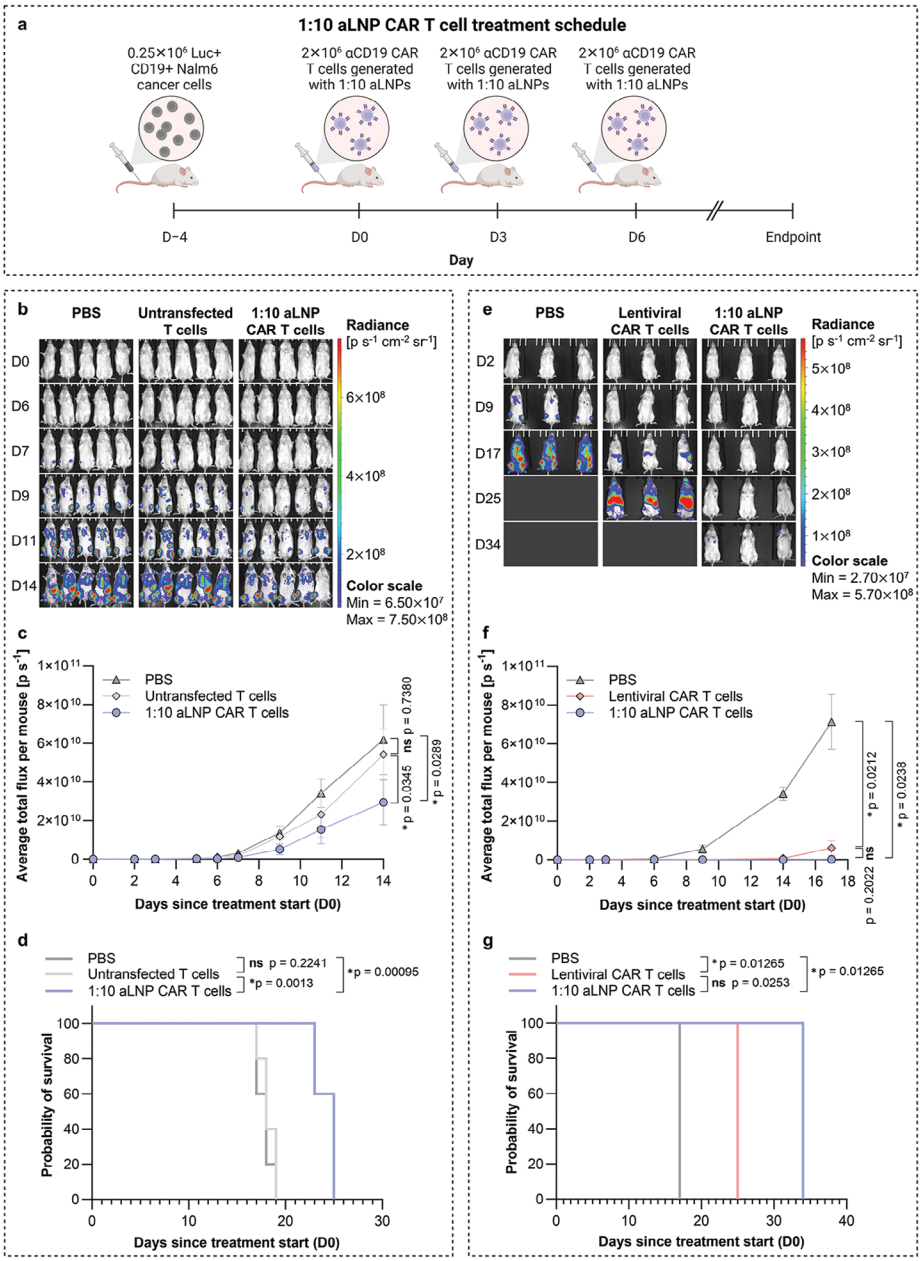

Figure 6. Adoptive transfer of anti-CD19 CAR T cells generated with aLNPs reduces tumor burden in a xenograft mouse model of leukemia. a) Schedule used to establish a low-leukemic burden in NSG mice followed by repeated treatments with CAR T cells generated with 1:10 aLNPs. b) Time-course IVIS images of Nalm6 (luciferase-expressing human leukemia) tumor-bearing NSG mice treated with three injections of PBS, untransfected T cells, or 1:10 aLNP generated CAR T cells. c) Time-course of quantification of average total flux per mouse for the images shown in panel (b). Data are presented as mean ± SD. Differences between all treatment means within each day were assessed by a two-way repeated measures ANOVA with post-hoc *t*-tests using Tukey's correction for multiple comparisons. Only comparisons for day 14 (the final imaging timepoint) are shown. $*p \leq 0.05$, ns = not significant. d) Kaplan–Meier survival curves of the mice following treatment. Differences between survival profiles were assessed using pairwise log-rank tests with Bonferroni corrections for multiple comparisons. To determine significance, the *p*-values shown (all one-tail) were compared to the Bonferroni-corrected α value of 0.0167. * indicates significance, ns = not significant. (b–d) represent data from a single experiment, for which $n = 5$ mice per group. e) Time-course IVIS images of Nalm6 tumor-bearing NSG mice treated with three injections of 1:10 aLNP generated CAR T cells or PBS, compared to mice treated with a single injection of lentiviral CAR T cells on day 0 (D0). f) Time-course of quantification of average total flux per mouse for the images shown in panel (e). Data are presented as mean ± SD. Differences between all treatment means within each day were assessed by a two-way repeated measures ANOVA with post-hoc *t*-tests using Tukey's correction for multiple comparisons. Only comparisons for day 17 (the last day all mice were alive) are shown. $*p \leq 0.05$, ns = not significant. g) Kaplan–Meier survival curves of the mice following treatment. Differences between survival profiles were assessed using pairwise log-rank tests with Bonferroni corrections for multiple comparisons. To determine significance, the *p*-values shown (one-tail for PBS vs aLNP and PBS vs lentiviral; two-tail for aLNP vs lentiviral) were compared to the Bonferroni-corrected α value of 0.0167. * indicates significance, ns = not significant. (e–g) represents data from a single experiment, for which $n = 3$ mice per group. (a) was created with BioRender.com.

In the future, aLNPs could be explored for additional therapeutic uses or further engineered to increase their capabilities. While this study used aLNPs to deliver CAR mRNA to human T cells ex vivo, aLNPs could be investigated for the in situ generation of mRNA CAR T cells. Moreover, because aLNPs activate T cells, they may have the potential to turn "cold" immune-suppressing tumors into "hot" immune-responsive tumors. aLNPs could also be used to deliver mRNA encoding proteins other than CARs, such as cytokines or growth factors to further promote T cell activation. Combination immunotherapies of checkpoint blockade antibodies and aLNPs delivering immune stimulatory cytokines may provide advantageous and synergistic anti-cancer immune activation. Furthermore, mRNA CAR T cells generated by aLNPs may have applications beyond cancer. For example, they may be useful for the treatment of autoimmune conditions such as systemic lupus erythematosus and myasthenia gravis, where risk tolerance is lower and prolonged B cell aplasia is likely not needed.

Moving forward, the aLNP platform is well-situated to support additional engineering development. As one example, aLNPs could be reformulated to encapsulate different cargoes, perhaps transposon systems for the generation of permanent lentiviral-like CAR T cells, or CRISPR-Cas9 systems for the production of MHC knockout "off-the-shelf" CAR T cells or PD-1 knockout checkpoint blockade resistant CAR T cells. Furthermore, it has been previously reported that driving T cell expansion with a greater proportion of CD3 than CD28 antibodies results in faster T cell differentiation and less memory formation.[71] For many applications, it may therefore be preferable to use high CD28 antibody ratios to achieve more memory formation. While our 1:10 aLNP does provide high CD28 stimulation, additional investigation into the optimal level of high CD28 stimulation may allow us to leverage T cell memory to use RNA to knock in a permanent CAR, effectively combining the benefits of mRNA CAR T cell therapy with the potency of viral CAR T cell therapy. Last, we note that, while we advanced aLNPs with a 1:10 ratio of CD3 to CD28 antibody fragments to our murine xenograft model (Figure 6), aLNPs with different ratios may be useful for additional goals in T cell engineering.

In summary, aLNPs–LNPs with surface-conjugated human CD3 and CD28 antibody fragments–combine the APC-mimetic nature of activating beads with the mRNA transfecting capabilities of LNPs. We show that aLNPs facilitate rapid, one-step activation and transfection of primary human T cells with mRNA and that the resulting CAR T cells decrease tumor burden in a murine xenograft model. aLNPs have the potential to reduce the complexity, cost, and time of mRNA CAR T cell production, and the platform is well-poised to support additional immunotherapy applications.

4. Experimental Section

Ionizable Lipid Synthesis: The C14-4 ionizable lipid was synthesized as previously described.[25,26] Seven equivalents of 1,2-epoxytetradecane (MilliporeSigma, Burlington, MA) were reacted with one equivalent of 2-{2-[4-(2-{[2-(2-aminoethoxy)ethyl] amino}ethyl)piperazin-1-yl]ethoxy}ethan-1-amine (Enamine, Kyiv, Ukraine) in ethanol for 2 days with vigorous stirring at 80 °C. Afterward, the product was concentrated using a Rotovap R-300 (Buchi, New Castle, DE) and resuspended in ethanol before being used to formulate the lipid nanoparticles (LNPs).

mRNA Synthesis: Firefly luciferase, mCherry, and EGFP mRNAs were synthesized via in vitro transcription as previously described.[59] Briefly, linearized plasmids encoding the codon-optimized protein sequences were used as templates for T7 RNA polymerase (Megascript, Ambion). In the transcription reactions, N1-methyl-pseudouridine-5′-triphosphate (m1Ψ, #N-1081, TriLink BioTechnologies, San Diego, CA) was substituted for uridine triphosphate and mRNAs were given 130 nucleotide-long 3′ poly(A) tails. Following transcription, RNAs were given 5′ Cap-1 with the m7G capping kit and 2′-O-methyltransferase (ScriptCap, CellScript). mRNAs were then purified via fast protein liquid chromatography (FPLC) with an Akta Purifier (GE Healthcare). The correct synthesis of mRNAs was confirmed by denaturing or native agarose gel electrophoresis before storage at −80 °C.

CAR mRNA was also synthesized via in vitro transcription. A linearized plasmid encoding a second-generation, human CD19-targeted CAR with a CD3ζ domain and a 4-1BB costimulatory domain followed by a 64 nucleotide-long 3′ poly(A) tail was used as the template for T7 RNA polymerase (New England Biolabs, Ipswich, MA, #E2040S). In the transcription reactions, N1-methyl-pseudouridine-5′-triphosphate (m1Ψ, #N-1081, TriLink BioTechnologies, San Diego, CA) was substituted for uridine triphosphate. Murine RNAse inhibitor (New England Biolabs, #M0314S) was added to prevent RNA degradation. Following transcription, the plasmid template was digested with DNase I (New England Biolabs, #M0303S), and RNA was purified using the Monarch RNA Cleanup Kit (500 µg) (New England Biolabs, #T2050L). Then, RNA was given 5′ Cap-1 using the vaccinia capping system (New England Biolabs #M2080S) and 2′-O-methyltransferase (New England Biolabs, #M0366) followed by a second purification using the Monarch RNA Cleanup Kit (500 µg) (New England Biolabs, #T2050L).

Maleimide-Lipid Nanoparticle (mal-LNP) Formulation: mal-LNPs were formulated by mixing an aqueous mRNA solution with an ethanol lipid solution in a microfluidic device. The microfluidic device uses groove structures to induce chaotic mixing which results in the formation of homogenous LNPs.[72,73] To form the aqueous phase, mRNA was resuspended in a 10 mM citrate buffer (pH = 3) at 1 mg mL^{-1}. To form the ethanol phase, C14-4, 1,2-dioleoyl-*sn*-glycero-3-phosphoethanolamine (DOPE, Avanti Polar Lipids, Alabaster, AL), cholesterol (MilliporeSigma), 1,2-dimyristoyl-*sn*-glycero-3-phosphoethanolamine-N-[methoxy(polyethylene glycol)-2000] (ammonium salt) (14:0 PEG2000 PE, Avanti Polar Lipids), and 1,2-distearoyl-sn-glycero-3-phosphoethanolamine-N-[maleimide(polyethylene glycol)-2000] (ammonium salt) (DSPE-PEG2000 Maleimide, Avanti Polar Lipids) were combined at molar percentages of 41% C14-4, 30.8% DOPE, 25.6% cholesterol, 2.1% C14-PEG2000, and 0.4% DSPE-PEG(2000) Maleimide. The aqueous and ethanol phases flowed into the microfluidic device at a 1:3 volume ratio (10:1 weight ratio of ionizable lipid:mRNA) using pump33DS syringe pumps (Harvard Apparatus, Holliston, MA). Upon exiting the device, mal-LNPs were dialyzed against PBS for 2 h at 20 kDa molecular weight cutoff. Care was taken to keep all materials ribonuclease (RNase) free. Dialysis was performed inside a biosafety cabinet for LNPs that were used to treat T cells administered to mice.

Antibody Cleavage and Disulfide Bond Reduction: Anti-human CD3 antibodies (BioXCell, InVivoMAb anti-human CD3, clone OKT-3, #BE0001-2) and anti-human CD28 antibodies (BioXCell, InVivoMAb anti-human CD28, clone 9.3, #BE0248) were cleaved with IdeZ protease (New England Biolabs, #P0770S) for 2 h at 37 °C with gentle shaking at 300 rpm. Following cleavage, dithiothreitol (DTT) was added directly to the cleavage reaction at a volume ratio of 1 µL 20 mM DTT per 40 µL reaction mixture to reduce disulfide bonds. The resulting mixture was incubated for 30 min at room temperature with gentle shaking at 300 rpm. Following incubation, reduced and cleaved antibody mixtures were diluted in PBS and concentrated on pre-wet 10 kDa spin columns (abcam, #ab93349) to remove DTT. Antibody cleavage was confirmed by denaturing gel electrophoresis.

aLNP Formulation: The cleaved, reduced, and concentrated CD3 and CD28 antibody mixtures were directly added to dialyzed mal-LNPs at a stoichiometric equivalent of one antibody fragment per 1 maleimide

binding site (≈3.5 fragments were assumed per whole antibody). Suspensions were mixed via pipetting and then were incubated for 1 h at room temperature with gentle shaking at 300 rpm. After incubation at room temperature, aLNPs were moved to 4 °C to finish reacting overnight with no shaking. The next day, aLNPs were purified by size exclusion chromatography with PBS as a running buffer (Sephadex G-75 beads, Sigma-Aldrich, St. Louis, MO, #G7550) to remove the unbound Fc fragments and any unbound Fd', LC, or F(ab') fragments.

LNP Characterization: LNPs were diluted 100X in 1X PBS. Dynamic light scattering was obtained using a Zetasizer Nano (Malvern Instruments, Malvern, UK) to measure polydispersity index (PDI) and hydrodynamic diameter (intensity-weighted Z-average) in triplicate. SD of the PDI was reported as the SD of the three measurements. SD of hydrodynamic diameter was calculated as SD = $\sqrt{(\text{average PDI} \times (\text{average Z-average})^2)}$. An Infinite 200 Pro M Plex plate reader with a NanoQuant plate (Tecan, Morrisville, NC) was used to ascertain the mRNA concentration of the LNPs by measuring absorbance at 260 nm.

RiboGreen Assay for Encapsulation Efficiency: A sample of each particle to be analyzed was diluted into either TE buffer or TE buffer containing 0.1% Triton X-100 (MilliporeSigma). After a 10-min incubation to allow the Triton X-100 to lyse the particles, the samples were transferred into a black 96-well plate in triplicate along with RNA standards. The Quant-iT RiboGreen reagent (Invitrogen #R11490) was added to all wells according to manufacturer protocol and fluorescence was analyzed using an Infinite 200 Pro M Plex plate reader (Tecan). A standard curve was generated to determine mRNA concentration in the lysed and non-lysed samples, and encapsulation efficiency was calculated as EE = (mRNA concentration in lysed sample − mRNA concentration in non-lysed sample)/mRNA concentration in lysed sample × 100.

Measurement of CD3 and CD28 Antibody Fragment Concentrations in 1:10 aLNP Preparation: Before conjugation to the mal-LNP surface, cleaved and reduced αCD3 and αCD28 antibody fragments were fluorescently labeled using DyLight Antibody Labeling Kits according to manufacturer protocols. αCD3 fragments were labeled with DyLight 550 (Thermo Scientific #84530) and αCD28 fragments were labeled with DyLight 755 (Thermo Scientific #84538). These spectrally distinct dyes were chosen to avoid spectral overlap. After overnight incubation with the dyed antibody fragments and size exclusion chromatography, dyed aLNPs were plated in triplicate in black 96 well plates alongside standards generated with free dyed αCD3 and αCD28 antibody fragments. Fluorescence was analyzed using an Infinite 200 Pro M Plex plate reader (Tecan) and standard curves were generated to determine αCD3 and αCD28 fragment concentrations. Undyed aLNPs were included as a negative control, with no background fluorescence detected.

Primary Human T Cell Culture: The Human Immunology Core (HIC) at the University of Pennsylvania obtained PBMCs from de-identified consenting healthy human donors by leukapheresis (under an Institutional Review Board-approved protocol) and used a negative selection process to sort the cells into subcategories. For this work, CD4+ and CD8+ T cells were obtained from the HIC and mixed in a 1:1 ratio in RPMI-1640 medium supplemented with L-glutamine (Gibco), 10% (v/v) FBS (Gibco), and 1% (v/v) penicillin-streptomycin (Gibco) and maintained in a 37 °C, 5% CO_2 humidified incubator. Control groups were activated with Dynabeads Human T-Activator CD3/CD28 (ThermoFisher, #11132D) using a 1:1 bead:cell ratio.

Nalm6 Cell Culture: The Nalm6 acute lymphoblastic leukemia human cells used in this study were kindly provided by Prof. Carl H. June at the University of Pennsylvania, who obtained the cells from ATCC (ATCC #CRL-3273) and transduced them to stably express click beetle green luciferase and GFP. Nalm6 cells were cultured in RPMI-1640 medium supplemented with L-glutamine (Gibco), 10% (v/v) FBS (Gibco), and 1% (v/v) penicillin-streptomycin (Gibco) and maintained in a 37 °C, 5% CO_2 humidified incubator. Cells were confirmed to be mycoplasma negative by the Cell Center Core at the University of Pennsylvania, which used the Cambrex MycoAlert Mycoplasma Detection Assay.

Luciferase mRNA Delivery to Primary Human T Cells Ex Vivo: Primary human T cells (bead-activated and non-activated) were plated in triplicate in clear-bottomed 96 well plates at 60 000 cells per 60 µL per well. LNPs (mal-LNPs, αCD3-LNPs, αCD28-LNPs, αCD3-LNPs + αCD28-LNPs, and aLNPs) were used to administer 200 ng of luciferase mRNA to each well. After 24 h, plates were centrifuged at 300 g for 7 min. Media was aspirated and cells were resuspended in 50 µL of 1X Reporter Lysis Buffer (Promega, Madison, WI, #E3971). 100 µL of Luciferase Assay Substrate (Promega, #E4550) was added in minimal light, and suspensions were mixed via pipette. After a 10-min dark incubation, an Infinite 200 Pro M Plex plate reader (Tecan) was used to measure the luminescent signal. For each primary cell donor, luminescence was normalized to that donor's untreated cells.

mCherry and EGFP mRNA Delivery to Primary Human T Cells Ex Vivo: Primary human T cells (bead-activated and non-activated) were plated in triplicate or quadruplicate in clear-bottomed 96 well plates at 60 000 cells per 60 µL per well. LNPs (mal-LNPs and 1:50, 1:10, 1:3, 1:1, 3:1, 10:1, and 50:1 aLNPs) were used to administer 200 ng of mCherry or EGFP mRNA to each well. After 24 h, plates were centrifuged at 300 g for 7 min. Media was aspirated and cells were washed and resuspended in PBS. Expression of mCherry or EGFP was assessed relative to an untreated control using a BD LSRII flow cytometer. Data were analyzed using FlowJo 10.5.3 software. Standard gating was applied with doublet exclusion.

Viability Assays: Primary human T cells (bead-activated and non-activated) were plated in triplicate in clear-bottomed 96 well plates at 60 000 cells per 60 µL per well. aLNPs were used to administer a fixed amount of mRNA to each well. After 24 h, 60 µL of CellTiter-Glo Luminescent Cell Viability Assay Reagent (Promega, #G7572) was added per well in minimal light, and suspensions were mixed via pipette. After a 10-min dark incubation, an Infinite 200 Pro M Plex plate reader (Tecan) was used to measure the luminescent signal. For each primary cell donor, luminescence (proportional to the amount of ATP–and therefore, to the number of cells–in the culture) was normalized to that donor's untreated cells.

Co-Culture of aLNP Generated CAR T Cells with Nalm6 Cells: Primary human T cells (bead-activated and non-activated) were plated in 6 well plates at a density of 1×10^6 cells per mL. LNPs (mal-LNPs and various aLNPs) were used to administer CD19-directed CAR mRNA at a dose of 400 ng mRNA per 60 000 cells in Figures 4e and 5c, or 600 ng mRNA per 60 000 cells in Figure 4f and Figure S6, Supporting Information. Media was supplemented with recombinant human IL-2 at 50 U μL^{-1} (Corning, #BD354043). After 24 h for Figure 4e,f, and Figure S6, Supporting Information, or after 4 days for Figure 5c, a sample of cells was removed from each group and centrifuged at 300 g for 7 min. Media was aspirated, cells were resuspended in PBS, and stained with a rabbit anti-mouse FMC63 scFv monoclonal antibody conjugated to PE (Cytoart, Tucson, AZ, #200105) which binds to the specific CAR we used. After staining, cells were washed and resuspended in PBS. CAR surface expression was assessed relative to an untreated control using a BD LSRII flow cytometer. Data were analyzed using FlowJo 10.5.3 software. Standard gating was applied with doublet exclusion.

After confirming cell-surface expression of CAR, CAR T cells (bead + mal-LNP generated or aLNP generated) were plated in co-culture with 25 000 Nalm6 (luciferase-expressing CD19+ human acute lymphoblastic leukemia) cells at various CAR T cell:Nalm6 cell ratios (1:1, 1:2, 1:4, 1:8, 1:16, 0:1) in triplicate in clear-bottomed 96-well plates; CAR+ cells were not sorted from total T cells, instead a number of total T cells scaled by the CAR positivity rate was plated.[21,25,26,74] After 48 h, plates were centrifuged at 300 g for 7 min. Media was aspirated and cells were resuspended in 50 µL of 1× Reporter Lysis Buffer (Promega, #E3971). 100 µL of Luciferase Assay Substrate (Promega, #E4550) was added in minimal light, and suspensions were mixed via pipette. After a 10-min dark incubation, an Infinite 200 Pro M Plex plate reader (Tecan) was used to measure the luminescent signal. The percent of Nalm6 cells killed per co-culture well was calculated as % = (luminescence of 0:1 well − luminescence of co-culture well)/luminescence of 0:1 well × 100.

CellTrace Far Red Proliferation Assay: Primary human T cells were stained with CellTrace Far Red (ThermoFisher, #C34564) according to manufacturer protocol. Immediately following staining, cells were plated in 6 well plates at a density of 1×10^6 cells per mL. A portion of the cells were activated with Dynabeads Human T-Activator CD3/CD28 (ThermoFisher, #11132D) using a 1:1 bead:cell ratio. mal-LNPs or

1:10 aLNPs were used to administer 400 ng of CAR mRNA per 60 000 cells to the bead-activated or non-activated cells, respectively. Media was supplemented with recombinant human IL-2 at 50 U μL^{-1} (Corning, Corning, NY, #BD354043) for all groups except the no treatment (NT) control. On days 2, 4, and 6 post-LNP administration, portions of the cultures were removed and centrifuged at 300 g for 7 min. Media was aspirated and cells were resuspended in PBS for analysis in duplicate relative to the NT control on a BD LSRII flow cytometer using a low flow rate to ensure separation of generational peaks. Data were analyzed using FlowJo 10.5.3 software. Standard gating was applied with doublet exclusion.

Analysis of Cell-Surface Activation Markers: Primary human T cells (bead-activated and non-activated) were plated in 6 well plates at a density of 1×10^6 cells per mL. mal-LNPs were used to administer 400 ng of CAR mRNA per 60 000 bead-activated cells (B+L). LNPs with only CD3 antibody fragments on their surface (αCD3), LNPs with only CD28 antibody fragments on their surface (αCD28), or 1:10 aLNPs (1:10) were used to administer 400 ng of CAR mRNA per 60 000 non-activated cells. Media was supplemented with recombinant human IL-2 at 50 U μL^{-1} (Corning, #BD354043) for all groups except the no treatment (NT) control. After 24 h, cells were centrifuged at 300 g for 7 min. Media was aspirated, cells were resuspended in PBS, and stained with PE anti-human CD25 (BioLegend, San Diego, CA, #302606), FITC anti-human CD44 (BioLegend, #397518), APC anti-human CD45RA (BioLegend, #304112), AF700 anti-human CCR7 (BioLegend, #353244), and APC-Cyanine7 anti-Human CD69 (BioLegend, #310914) according to manufacturer protocols. After staining, cells were washed, resuspended in PBS, and further stained with SYTOX Blue Dead Cell Stain (ThermoFisher, #S34857) according to manufacturer protocol. Surface expression of CD25, CD69, CD44, CCR7, and CD45RA was assessed in quadruplicate using a BD LSRII flow cytometer. Unstained and single stain controls were used for compensation; fluorescence minus one controls were used to accurately define the positive populations. Data were analyzed using FlowJo 10.5.3 software. Standard gating was applied with the exclusion of doublets and dead (SYTOX positive) cells.

To further investigate CCR7 and CD45RA expression at a later time point, primary human T cells (bead-activated and non-activated) were plated in 12 well plates at a density of 1×10^6 cells per mL. mal-LNPs were used to administer 400 ng of CAR mRNA per 60 000 bead-activated cells (B+L) and 1:10 aLNPs were used to administer 400 ng of CAR mRNA per 60 000 non-activated cells. Media was supplemented with recombinant human IL-2 at 50 U μL^{-1} (Corning, #BD354043). After 3 days, cells were centrifuged at 300 g for 7 min. Media was aspirated, cells were resuspended in PBS and stained with APC/Cyanine7 anti-human CCR7 (BioLegend, #353212) and Brilliant Violet 421 anti-human CD45RA (BioLegend, #304130) according to manufacturer protocols. After staining, cells were washed, resuspended in PBS, and further stained with ViaKrome 808 Fixable Viability Dye (Beckman Coulter, #C36628) according to manufacturer protocol. Surface expression of CCR7 and CD45RA was analyzed in triplicate using a BD LSRII flow cytometer. Unstained and single-stain controls were used for compensation. Data were analyzed using FlowJo 10.5.3 software. Standard gating was applied with the exclusion of doublets and dead cells.

ELISA Quantification of Granzyme B, Perforin, Soluble FasL, TNFα, and IFNγ: Primary human T cells (bead-activated and non-activated) were plated in 6 well plates at a density of 1×10^6 cells per mL. mal-LNPs were used to administer 400 ng of CAR mRNA per 60 000 bead-activated cells (B+L). LNPs with only CD3 antibody fragments on their surface (αCD3), LNPs with only CD28 antibody fragments on their surface (αCD28), or 1:10 aLNPs (1:10) were used to administer 400 ng of CAR mRNA per 60 000 non-activated cells. Media was supplemented with recombinant human IL-2 at 50 U μL^{-1} (Corning, #BD354043) for all groups except the NT control. After 24 h, supernatants were collected and stored at −80 °C until the time of analysis. Invitrogen ELISA kits were used to quantify granzyme B, perforin, soluble FasL, TNFα, and IFNγ concentrations (Invitrogen #BMS2027-2, #BMS2306, #BMS260-2, #KHC3011, and #KHC4021, respectively) following manufacturer protocols with an Infinite 200 Pro M Plex plate reader (Tecan).

Small Molecule Mechanism of Uptake Study: Before LNP treatment, primary human T cells (1:1 mixture of CD4+ and CD8+) were incubated for 30 min with 100 µM Dynasore (inhibitor of dynamic endocytosis, i.e., both clathrin-mediated and caveolae-mediated endocytosis), 5 mM methyl-β-cyclodextrin (MβCD, inhibitor of lipid raft-mediated endocytosis), 200 µM genistein (inhibitor of caveolae-mediated endocytosis), 20 µM chlorpromazine (CMZ, inhibitor of clathrin-mediated endocytosis), or 2 mM amiloride (inhibitor of macropinocytosis).[75,76] Following incubation, cells were pelleted and resuspended in a fresh RPMI-1640 medium. A portion of the cells was activated with beads before cells were plated in triplicate in a clear-bottomed 96-well plate at 100 000 cells per 100 µL per well. mal-LNPs and 1:10 aLNPs were used, respectively, to administer 670 ng of luciferase mRNA to each well of bead-activated or non-activated cells. After 24 h, Luciferase Assay Substrate (Promega, #E4550) was added and the luminescent signal was measured.

Fab Blocking Study: Fluorescently labeled mal-LNPs and 1:10 aLNPs encapsulating EGFP mRNA were prepared by mixing the lipid-like fluorescent dye 1,1′-dioctadecyl-3,3,3′,3′-tetramethylindotricarbocyanine iodide (DiR) at 1 mol % of total lipids with LNPs prior to dialysis. Separately, anti-human CD3 antibodies (BioXCell, #BE0001-2) and anti-human CD28 antibodies (BioXCell, #BE0248) were cleaved into Fabs and purified with the Pierce Fab Micro Preparation Kit (ThermoFisher, #44685) following the manufacturer's protocol. Primary human T cells (1:1 mixture of CD4+ and CD8+) were incubated for 1 h with 250 ng αCD3 Fabs and 250 ng αCD28 Fabs per million cells per mL to block binding of beads or aLNPs to CD3/CD28 on the T cell surface. Following Fab incubation, a portion of the cells was treated with activating beads before cells were plated in a 6-well plate at a density of 1×10^6 cells per mL. DiR mal-LNPs or DiR 1:10 aLNPs were used, respectively, to administer 400 ng of EGFP mRNA per 60 000 cells to bead-treated or untreated cells. Non-Fab blocked groups were included as controls. After 24 h, DiR (LNP uptake) and EGFP (cargo mRNA expression) fluorescence were analyzed via flow cytometry relative to an unblocked untreated control (with standard gating and doublet exclusion).

In Vivo Leukemia Xenograft Model: In order to obtain enough T cells for this experiment, primary female human T cells procured from the HIC at Penn were expanded: on day −5, a 1:1 mixture of CD4+:CD8+ T cells was plated at a density of 1×10^6 cells per mL with recombinant human IL-2 at 50 U/µL (Corning, #BD354043) and Dynabeads Human T-Activator CD3/CD28 at a 1:1 bead:cell ratio. On day −1 (after 4 days of expansion), beads were removed with a MojoSort magnet and 1:10 aLNPs were used to administer 400 ng of CAR mRNA per 60 000 cells to a portion of the cells. After 24 h (day 0), samples of aLNP-treated and aLNP-untreated cells were removed and centrifuged at 300 g for 7 min. Media was aspirated, cells were resuspended in PBS, and stained with a rabbit anti-mouse FMC63 scFv monoclonal antibody conjugated to PE (Cytoart, #200105). After staining, cells were washed and resuspended in PBS. CAR surface expression was assessed relative to an untreated control using a BD LSRII flow cytometer in triplicate. Data were analyzed using FlowJo 10.5.3 software. Standard gating was applied with doublet exclusion.

Concurrently, on day −4, 250 000 luciferase-expressing CD19+ Nalm6 cells were injected in 100 µL sterile PBS into the tail veins of female 8–10-week-old NOD.Cg-Prkdc^{scid}Il2rg^{tm1Wjl}/SzJ (NSG) mice. On day 0, after confirming the establishment of similar tumor burden in all mice and randomly allocating them into groups, 2×10^6 CAR T cells generated with 1:10 aLNPs were administered in 100 µL sterile PBS via tail vein injection to five mice; CAR+ cells were not sorted from total T cells, instead, a number of total T cells scaled by the CAR positivity rate was administered. Furthermore, prior to infusion, CAR T cells that were generated with aLNPs were centrifuged at 300 g, washed, and resuspended in 1× PBS. Therefore, the authors did not expect that any appreciable amount of aLNPs was transferred along with the CAR T cells into the mice. As control groups, five mice received tail vein injections of untransfected T cells, and five mice received tail vein injections of PBS. On days 2 and 5, 1:10 aLNPs were used to transfect fresh CAR T cells (from the original culture of primary human T cells). On days 3 and 6, after confirming CAR expression by flow cytometry, aLNP CAR T cells, untransfected T cells, and PBS were re-injected.

Periodically throughout the treatment, mice were intraperitoneally injected with 200 µL of *D*-luciferin potassium salt (Biotium, Fremont, CA) in PBS at 15 mg mL^{-1}. After 10 min, mice were anesthetized with 2.5%

isoflurane and a Lumina S3 in vivo imaging system (IVIS, PerkinElmer, Waltham, MA) was used to capture bioluminescence images. Living Image 4.7.3 Software (PerkinElmer) was used to quantify the total flux for each mouse at each imaging time point. After day 14, mice were monitored for survival and euthanized with CO_2 at the first sign of illness. The mice were bred and housed, and all animal work was done at the Stem Cell and Xenograft Core (RRID:SCR_010035) at the University of Pennsylvania to maintain a sterile environment, under a protocol approved by the University of Pennsylvania's Institutional Animal Care and Use Committee (IACUC protocol #806540). The animal housing facility was maintained at 22 ± 2 °C, 12-h dark/light cycle, and 40–70% air humidity.

The second leukemia xenograft experiment (Figure 6e–g) was conducted in a similar manner, using $n = 3$ mice, with no changes in methodology for the PBS and 1:10 aLNP CAR T cell treated groups. For the lentiviral CAR T cell group, on day −1, cryopreserved lentiviral CAR T cells were thawed into RPMI medium at a density of 1×10^6 cells per mL. After 24 h (day 0), a portion of the thawed cells was removed and centrifuged at 300 g for 7 min. Media was aspirated, cells were resuspended in PBS, and stained with a rabbit anti-mouse FMC63 scFv monoclonal antibody conjugated to PE (Cytoart, #200105). After staining, cells were washed and resuspended in PBS. CAR surface expression was assessed relative to an untransfected control using a BD LSRII flow cytometer. Data were analyzed using FlowJo 10.5.3 software. Standard gating was applied with doublet exclusion. After confirming CAR expression, each mouse received a single injection of 1×10^6 lentiviral CAR T cells in 100 µL sterile PBS via tail vein injection. CAR+ cells were not sorted from total T cells, instead, a quantity of total T cells scaled by the CAR positivity rate was administered.

Lentiviral CAR T Cell Production: Lentiviral vector production was performed as previously described.[77,78] HEK293T cells were transfected with the 4-1BB-based CD19-targeting CAR and lentiviral packaging plasmids using Lipofectamine 2000 (Invitrogen) following the manufacturer's protocol. Lentiviral supernatants were collected at 24 and 48 h after transfection and concentrated using high-speed ultracentrifugation. To generate lentiviral stocks, the resulting concentrated lentivirus batches were resuspended in cold R10 media and stored at −80 °C.

Primary human CD4+ and CD8+ T cells were combined at a 1:1 ratio and activated with CTS Dynabeads CD3/CD28 (ThermoFisher) at a 3:1 bead-to-cell ratio at 1×10^6 cells per mL. After 24 h, T cells were transduced at a multiplicity of infection (MOI) of 3 lentivirus particles per cell. After 5 days, beads were removed from cultures. T cell cultures were maintained at 6×10^5 cells per mL. Cell number and volume were monitored daily using a Multisizer 3 Coulter Counter (Beckman). Transduced T cells were cryopreserved when they reached a rested state, as determined by cell volume.

Statistical Analysis: Data were presented as mean ± SD. Differences between means were assessed by ordinary or repeated measures of one-way or two-way analyses of variance (ANOVAs) with post-hoc *t*-tests using Tukey's, Šídák's, or Dunnett's correction for multiple comparisons. Differences between survival profiles were assessed using pairwise log-rank tests with Bonferroni corrections for multiple comparisons. Statistical analyses were completed using GraphPad Prism 9.5.1 with significance level $\alpha = 0.05$.

Supporting Information

Supporting Information is available from the Wiley Online Library or from the author.

Acknowledgements

M.J.M. acknowledges support from a US National Institutes of Health Director's New Innovator Award (DP2 TR002776), a Burroughs Wellcome Fund Career Award at the Scientific Interface (CASI), a US National Science Foundation CAREER award (CBET-2145491), and an American Cancer Society Research Scholar Grant (RSG-22-122-01-ET). N.C.S. acknowledges grant support from the Emerson Collective. A.E.M., C.G.F.-E., A.S.T., R.M.H., A.J.M., and A.G.H. were supported by US National Science Foundation Graduate Research Fellowships. M.M.B. was supported by a US National Institutes of Health Ruth L. Kirschstein National Research Service Award (F31CA260922). M.S.P. was supported by the National Institute of Dental and Craniofacial Research of the US National Institutes of Health (T90DE030854). D.M. was supported by the University of Pennsylvania Fontaine Fellowship, the Norman and Selma Kron Research Fellowship, and the Robert Wood Johnson Foundation Health Policy Research Scholars Program. The authors thank Lynn Chen, Max Eldabbas, and Emileigh Maddox of the Human Immunology Core (HIC) at the Perelman School of Medicine at the University of Pennsylvania (RRID: SCR_022380) for assistance with primary human T cell procurement. The HIC is supported in part by NIH P30 AI045008 and P30 CA016520.

Conflict of Interest

A.E.M., M.M.B., and M.J.M. are inventors on a patent filed by the Trustees of the University of Pennsylvania (US Provisional Patent Application No. 63/378,819, filed October 7, 2022; PCT International Patent Application No. PCT/US23/76231, filed October 6, 2023) describing the CD3/CD28 antibody fragment conjugated lipid nanoparticle technology described in this work. NCS holds equity in Tmunity Therapeutics and is an advisor to Tome Biosciences. All other authors declare they have no competing interests.

Author Contributions

M.S.P., N.G., and M.M.B. contributed equally to this work. A.E.M., M.M.B., N.G., M.S.P., M.M., X.H., C.G.F.-E., R.M.H., A.J.M., and M.J.M. conceived and designed the experiments. A.E.M., M.M.B., M.S.P., N.G., X.H., M.M., D.M., C.G.F.-E., A.S.T., and A.G.H. performed the experiments. A.E.M. and M.M.B. analyzed the data. A.E.M. wrote the manuscript and prepared the figures. M.J.M., M.S.P., M.M.B., D.M., N.C.S, C.H.J., M.-G.A., and D.W. reviewed and edited the manuscript. M.J.M., N.C.S, C.H.J., and D.W. supervised the entire project. All authors approved the final manuscript for submission.

Data Availability Statement

The data that support the findings of this study are available from the corresponding author upon reasonable request.

Keywords

biomimicry, cancer immunotherapy, CAR T cells, lipid nanoparticles, mRNA

Received: December 5, 2023
Revised: February 5, 2024
Published online:

[1] FDA Approval Brings First Gene Therapy to the United States, FDA, **2020**, https://www.fda.gov/news-events/press-announcements/fda-approval-brings-first-gene-therapy-united-states.
[2] FDA Approves CAR-T Cell Therapy to Treat Adults with Certain Types of Large B-Cell Lymphoma, FDA, **2020**, https://www.fda.gov/news-events/press-announcements/fda-approves-car-t-cell-therapy-treat-adults-certain-types-large-b-cell-lymphoma.
[3] FDA Approves First Cell-Based Gene Therapy For Adult Patients with Relapsed or Refractory MCL, FDA, **2020**.

[4] FDA D. I. S. C. O., Burst Edition: FDA Approval of Breyanzi (Lisocabtagene Maraleucel) for Second-Line Treatment of Large B-Cell Lymphoma, FDA, **2022**, https://www.fda.gov/news-events/press-announcements/fda-approves-first-cell-based-gene-therapy-adult-patients-relapsed-or-refractory-mcl.
[5] FDA D. I. S. C. O., Burst Edition: FDA Approval of ABECMA (Idecabtagene Vicleucel) the First FDA Approved Cell-Based Gene Therapy for the Treatment of Adult Patients with Relapsed or Refractory Multiple Myeloma, FDA, **2021**.
[6] FDA D. I. S. C. O., Burst Edition: FDA Approval of CARVYKTI (Ciltacabtagene Autoleucel) for the Treatment of Adult Patients with Relapsed or Refractory Multiple Myeloma after Four or More Prior Lines of Therapy, Including a Proteasome Inhibitor, an Immunomodulatory Agent, and an Anti-CD38 Monoclonal Antibody, FDA, **2022**.
[7] L. Labanieh, C. L. Mackall, *Nature* **2023**, *614*, 635.
[8] C. E. Brown, D. Alizadeh, R. Starr, L. Weng, J. R. Wagner, A. Naranjo, J. R. Ostberg, M. S. Blanchard, J. Kilpatrick, J. Simpson, A. Kurien, S. J. Priceman, X. Wang, T. L. Harshbarger, M. D'Apuzzo, J. A. Ressler, M. C. Jensen, M. E. Barish, M. Chen, J. Portnow, S. J. Forman, B. Badie, *N. Engl. J. Med.* **2016**, *375*, 2561.
[9] D. M. O'Rourke, M. P. Nasrallah, A. Desai, J. J. Melenhorst, K. Mansfield, J. J. D. Morrissette, M. Martinez-Lage, S. Brem, E. Maloney, A. Shen, R. Isaacs, S. Mohan, G. Plesa, S. F. Lacey, J.-M. Navenot, Z. Zheng, B. L. Levine, H. Okada, C. H. June, J. L. Brogdon, M. V. Maus, *Sci. Transl. Med.* **2017**, *9*, aaa0984.
[10] H. Li, Y. Huang, D.-Q. Jiang, L.-Z. Cui, Z. He, C. Wang, Z.-W. Zhang, H.-L. Zhu, Y.-M. Ding, L.-F. Li, Q. Li, H.-J. Jin, Q.-J. Qian, *Cell Death Dis.* **2018**, *9*, 177.
[11] C. R. Maldini, D. T. Claiborne, K. Okawa, T. Chen, D. L. Dopkin, X. Shan, K. A. Power, R. T. Trifonova, K. Krupp, M. Phelps, V. D. Vrbanac, S. Tanno, T. Bateson, G. J. Leslie, J. A. Hoxie, C. L. Boutwell, J. L. Riley, T. M. Allen, *Nat. Med.* **2020**, *26*, 1776.
[12] J. G. Rurik, I. Tombácz, A. Yadegari, P. O. Méndez Fernández, S. V. Shewale, L. Li, T. Kimura, O. Y. Soliman, T. E. Papp, Y. K. Tam, B. L. Mui, S. M. Albelda, E. Puré, C. H. June, H. Aghajanian, D. Weissman, H. Parhiz, J. A. Epstein, *Science* **2022**, *375*, 91.
[13] R. C. Larson, M. V. Maus, *Nat. Rev. Cancer* **2021**, *21*, 145.
[14] M. Namuduri, R. J. Brentjens, *Expert Rev. Hematol.* **2016**, *9*, 511.
[15] C. L. Bonifant, H. J. Jackson, R. J. Brentjens, K. J. Curran, *Mol. Ther.–Oncolytics* **2016**, *3*, 16011.
[16] M.-L. Schubert, M. Schmitt, L. Wang, C. A. Ramos, K. Jordan, C. Müller-Tidow, P. Dreger, *Ann. Oncol.* **2021**, *32*, 34.
[17] T. Giavridis, S. J. C. van der Stegen, J. Eyquem, M. Hamieh, A. Piersigilli, M. Sadelain, *Nat. Med.* **2018**, *24*, 731.
[18] S. L. Maude, N. Frey, P. A. Shaw, R. Aplenc, D. M. Barrett, N. J. Bunin, A. Chew, V. E. Gonzalez, Z. Zheng, S. F. Lacey, Y. D. Mahnke, J. J. Melenhorst, S. R. Rheingold, A. Shen, D. T. Teachey, B. L. Levine, C. H. June, D. L. Porter, S. A. Grupp, *N. Engl. J. Med.* **2014**, *371*, 1507.
[19] J. J. Melenhorst, G. M. Chen, M. Wang, D. L. Porter, C. Chen, M. A. Collins, P. Gao, S. Bandyopadhyay, H. Sun, Z. Zhao, S. Lundh, I. Pruteanu-Malinici, C. L. Nobles, S. Maji, N. V. Frey, S. I. Gill, A. W. Loren, L. Tian, I. Kulikovskaya, M. Gupta, D. E. Ambrose, M. M. Davis, J. A. Fraietta, J. L. Brogdon, R. M. Young, A. Chew, B. L. Levine, D. L. Siegel, C. Alanio, E. J. Wherry, et al., *Nature* **2022**, *602*, 503.
[20] J. Wat, S. Barmettler, *J. Allergy Clin. Immunol.: Pract.* **2022**, *10*, 460.
[21] D. M. Barrett, Y. Zhao, X. Liu, S. Jiang, C. Carpenito, M. Kalos, R. G. Carroll, C. H. June, S. A. Grupp, *Hum. Gene Ther.* **2011**, *22*, 1575.
[22] H. Almåsbak, E. Walseng, A. Kristian, M. R. Myhre, E. M. Suso, L. A. Munthe, J. T. Andersen, M. Y. Wang, G. Kvalheim, G. Gaudernack, J. A. Kyte, *Gene Ther.* **2015**, *22*, 391.
[23] J. B. Foster, N. Choudhari, J. Perazzelli, J. Storm, T. J. Hofmann, P. Jain, P. B. Storm, N. Pardi, D. Weissman, A. J. Waanders, S. A. Grupp, K. Karikó, A. C. Resnick, D. M. Barrett, *Hum. Gene Ther.* **2019**, *30*, 168.
[24] N. N. Parayath, S. B. Stephan, A. L. Koehne, P. S. Nelson, M. T. Stephan, *Nat. Commun.* **2020**, *11*, 6080.
[25] M. M. Billingsley, N. Singh, P. Ravikumar, R. Zhang, C. H. June, M. J. Mitchell, *Nano Lett.* **2020**, *20*, 1578.
[26] M. M. Billingsley, A. G. Hamilton, D. Mai, S. K. Patel, K. L. Swingle, N. C. Sheppard, C. H. June, M. J. Mitchell, *Nano Lett.* **2022**, *22*, 533.
[27] T. Soundara Rajan, A. Gugliandolo, P. Bramanti, E. Mazzon, *Int. J. Mol. Sci.* **2020**, *21*, 6514.
[28] A. N. Miliotou, L. C. Papadopoulou, in *Chimeric Antigen Receptor T Cells: Development and Production*, (Eds.: K. Swiech, K. C. R. Malmegrim, V. Picanço-Castro), Springer, New York **2020**, pp. 87–117.
[29] N. Singh, X. Liu, J. Hulitt, S. Jiang, C. H. June, S. A. Grupp, D. M. Barrett, Y. Zhao, *Cancer Immunol. Res.* **2014**, *2*, 1059.
[30] Y. Zhao, E. Moon, C. Carpenito, C. M. Paulos, X. Liu, A. L. Brennan, A. Chew, R. G. Carroll, J. Scholler, B. L. Levine, S. M. Albelda, C. H. June, *Cancer Res.* **2010**, *70*, 9053.
[31] G. L. Beatty, A. R. Haas, M. V. Maus, D. A. Torigian, M. C. Soulen, G. Plesa, A. Chew, Y. Zhao, B. L. Levine, S. M. Albelda, M. Kalos, C. H. June, *Cancer Immunol. Res.* **2014**, *2*, 112.
[32] L. Raes, S. C. De Smedt, K. Raemdonck, K. Braeckmans, *Biotechnol. Adv.* **2021**, *49*, 107760.
[33] Phase I Clinical Trial of Autologous Mesothelin Re-Directed T Cells in Patients With Chemotherapy Refractory Metastatic Pancreatic Cancer, NCT01897415, Clinicaltrials.Gov, **2017**.
[34] G. L. Beatty, M. H. O'Hara, S. F. Lacey, D. A. Torigian, F. Nazimuddin, F. Chen, I. M. Kulikovskaya, M. C. Soulen, M. McGarvey, A. M. Nelson, W. L. Gladney, B. L. Levine, J. J. Melenhorst, G. Plesa, C. H. June, *Gastroenterology* **2018**, *155*, 29.
[35] Phase 1 Clinical Trial of Autologous Mesothelin Re-Directed T Cells Administered Intravenously in Patients With Progressive Malignant Pleural Mesothelioma, NCT01355965, Clinicaltrials.Gov, **2017**.
[36] Clinical Trial of Autologous cMet Redirected T Cells Administered Intratumorally in Patients With Breast Cancer, NCT01837602, Clinicaltrials.Gov, **2018**.
[37] J. Tchou, Y. Zhao, B. L. Levine, P. J. Zhang, M. M. Davis, J. J. Melenhorst, I. Kulikovskaya, A. L. Brennan, X. Liu, S. F. Lacey, A. D. Posey Jr., A. D. Williams, A. So, J. R. Conejo-Garcia, G. Plesa, R. M. Young, S. McGettigan, J. Campbell, R. H. Pierce, J. M. Matro, A. M. DeMichele, A. S. Clark, L. J. Cooper, L. M. Schuchter, R. H. Vonderheide, C. H. June, *Cancer Immunol. Res.* **2017**, *5*, 1152.
[38] Y. Zhao, Z. Zheng, C. J. Cohen, L. Gattinoni, D. C. Palmer, N. P. Restifo, S. A. Rosenberg, R. A. Morgan, *Mol. Ther.* **2006**, *13*, 151.
[39] T. DiTommaso, J. M. Cole, L. Cassereau, J. A. Buggé, J. L. S. Hanson, D. T. Bridgen, B. D. Stokes, S. M. Loughhead, B. A. Beutel, J. B. Gilbert, K. Nussbaum, A. Sorrentino, J. Toggweiler, T. Schmidt, G. Gyuelveszi, H. Bernstein, A. Sharei, *Proc. Natl. Acad. Sci. U. S. A.* **2018**, *115*, E10907.
[40] M. J. Mitchell, M. M. Billingsley, R. M. Haley, M. E. Wechsler, N. A. Peppas, R. Langer, *Nat. Rev. Drug Discovery* **2021**, *20*, 101.
[41] A. J. Mukalel, R. S. Riley, R. Zhang, M. J. Mitchell, *Cancer Lett.* **2019**, *458*, 102.
[42] X. Hou, T. Zaks, R. Langer, Y. Dong, *Nat. Rev. Mater.* **2021**, *6*, 1078.
[43] X. Han, H. Zhang, K. Butowska, K. L. Swingle, M.-G. Alameh, D. Weissman, M. J. Mitchell, *Nat. Commun.* **2021**, *12*, 7233.
[44] N. Chaudhary, D. Weissman, K. A. Whitehead, *Nat. Rev. Drug Discovery* **2021**, *20*, 817.
[45] A. D. Waldman, J. M. Fritz, M. J. Lenardo, *Nat. Rev. Immunol.* **2020**, *20*, 651.
[46] A. Trickett, Y. L. Kwan, *J. Immunol. Methods* **2003**, *275*, 251.
[47] J. C. Sunshine, J. J. Green, *Nanomedicine* **2013**, *8*, 1173.
[48] K. Perica, A. De León Medero, M. Durai, Y. L. Chiu, J. G. Bieler, L. Sibener, M. Niemöller, M. Assenmacher, A. Richter, M. Edidin,

M. Oelke, J. Schneck, *Nanomed.: Nanotechnol., Biol. Med.* **2014**, *10*, 119.
[49] J. C. Sunshine, K. Perica, J. P. Schneck, J. J. Green, *Biomaterials* **2014**, *35*, 269.
[50] R. A. Meyer, J. C. Sunshine, J. J. Green, *Trends Biotechnol.* **2015**, *33*, 514.
[51] R. A. Meyer, J. C. Sunshine, K. Perica, A. K. Kosmides, K. Aje, J. P. Schneck, J. J. Green, *Small* **2015**, *11*, 1519.
[52] M. P. Poltorak, P. Graef, C. Tschulik, M. Wagner, V. Cletiu, S. Dreher, B. Borjan, S. P. Fraessle, M. Effenberger, M. Turk, D. H. Busch, J. Plitzko, D. G. Kugler, S. Ragan, T. Schmidt, C. Stemberger, L. Germeroth, *Sci. Rep.* **2020**, *10*, 17832.
[53] E. Ben-Akiva, J. W. Hickey, R. A. Meyer, A. Isser, S. R. Shannon, N. K. Livingston, K. R. Rhodes, A. K. Kosmides, T. R. Warren, S. Y. Tzeng, J. P. Schneck, J. J. Green, *Acta Biomater.* **2023**, *160*, 187.
[54] K. J. Kauffman, J. R. Dorkin, J. H. Yang, M. W. Heartlein, F. DeRosa, F. F. Mir, O. S. Fenton, D. G. Anderson, *Nano Lett.* **2015**, *15*, 7300.
[55] S. Ramishetti, R. Kedmi, M. Goldsmith, F. Leonard, A. G. Sprague, B. Godin, M. Gozin, P. R. Cullis, D. M. Dykxhoorn, D. Peer, *ACS Nano* **2015**, *9*, 6706.
[56] D. Schmid, C. G. Park, C. A. Hartl, N. Subedi, A. N. Cartwright, R. B. Puerto, Y. Zheng, J. Maiarana, G. J. Freeman, K. W. Wucherpfennig, D. J. Irvine, M. S. Goldberg, *Nat. Commun.* **2017**, *8*, 1747.
[57] I. Tombácz, D. Laczkó, H. Shahnawaz, H. Muramatsu, A. Natesan, A. Yadegari, T. E. Papp, M.-G. Alameh, V. Shuvaev, B. L. Mui, Y. K. Tam, V. Muzykantov, N. Pardi, D. Weissman, H. Parhiz, *Mol. Ther.* **2021**, *29*, 3293.
[58] M. A. Oberli, A. M. Reichmuth, J. R. Dorkin, M. J. Mitchell, O. S. Fenton, A. Jaklenec, D. G. Anderson, R. Langer, D. Blankschtein, *Nano Lett.* **2017**, *17*, 1326.
[59] K. T. Love, K. P. Mahon, C. G. Levins, K. A. Whitehead, W. Querbes, J. R. Dorkin, J. Qin, W. Cantley, L. L. Qin, T. Racie, M. Frank-Kamenetsky, K. N. Yip, R. Alvarez, D. W. Y. Sah, A. de Fougerolles, K. Fitzgerald, V. Koteliansky, A. Akinc, R. Langer, D. G. Anderson, *Proc. Natl. Acad. Sci. U. S. A.* **2010**, *107*, 1864.
[60] N. Pardi, S. Tuyishime, H. Muramatsu, K. Kariko, B. L. Mui, Y. K. Tam, T. D. Madden, M. J. Hope, D. Weissman, *J. Controlled Release* **2015**, *217*, 345.
[61] A. J. Walker, R. G. Majzner, L. Zhang, K. Wanhainen, A. H. Long, S. M. Nguyen, P. Lopomo, M. Vigny, T. J. Fry, R. J. Orentas, C. L. Mackall, *Mol. Ther.* **2017**, *25*, 2189.
[62] K. L. Swingle, H. C. Safford, H. C. Geisler, A. G. Hamilton, A. S. Thatte, M. M. Billingsley, R. A. Joseph, K. Mrksich, M. S. Padilla, A. A. Ghalsasi, M.-G. Alameh, D. Weissman, M. J. Mitchell, *J. Am. Chem. Soc.* **2023**, *145*, 4691.
[63] J. Heyes, L. Palmer, K. Bremner, I. MacLachlan, *J. Controlled Release* **2005**, *107*, 276.
[64] M. Schmueck-Henneresse, B. Omer, T. Shum, H. Tashiro, M. Mamonkin, N. Lapteva, S. Sharma, L. Rollins, G. Dotti, P. Reinke, H.-D. Volk, C. M. Rooney, *J. Immunol.* **2017**, *199*, 348.
[65] D. Cibrián, F. Sánchez-Madrid, *Eur. J. Immunol.* **2017**, *47*, 946.
[66] S. Oehen, K. Brduscha-Riem, *J. Immunol.* **1998**, *161*, 5338.
[67] J. C. Charpentier, D. Chen, P. E. Lapinski, J. Turner, I. Grigorova, J. A. Swanson, P. D. King, *Nat. Commun.* **2020**, *11*, 180.
[68] J. C. Charpentier, P. D. King, *Cell Commun. Signaling* **2021**, *19*, 92.
[69] I. Evnouchidou, V. Caillens, D. Koumantou, L. Saveanu, *Biomed. J.* **2022**, *45*, 310.
[70] A. P. Jurgens, B. Popović, M. C. Wolkers, *Eur. J. Immunol.* **2021**, *51*, 2178.
[71] S. A. Grupp, M. Kalos, D. Barrett, R. Aplenc, D. L. Porter, S. R. Rheingold, D. T. Teachey, A. Chew, B. Hauck, J. F. Wright, M. C. Milone, B. L. Levine, C. H. June, *N. Engl. J. Med.* **2013**, *368*, 1509.
[72] D. Kalamasz, S. A. Long, R. Taniguchi, J. H. Buckner, R. J. Berenson, M. Bonyhadi, *J. Immunother.* **2004**, *27*, 405.
[73] D. Chen, K. T. Love, Y. Chen, A. A. Eltoukhy, C. Kastrup, G. Sahay, A. Jeon, Y. Dong, K. A. Whitehead, D. G. Anderson, *J. Am. Chem. Soc.* **2012**, *134*, 6948.
[74] S. J. Shepherd, C. C. Warzecha, S. Yadavali, R. El-Mayta, M.-G. Alameh, L. Wang, D. Weissman, J. M. Wilson, D. Issadore, M. J. Mitchell, *Nano Lett.* **2021**, *21*, 5671.
[75] M. Castella, A. Boronat, R. Martín-Ibáñez, V. Rodríguez, G. Suñé, M. Caballero, B. Marzal, L. Pérez-Amill, B. Martín-Antonio, J. Castaño, C. Bueno, O. Balagué, E. A. González-Navarro, C. Serra-Pages, P. Engel, R. Vilella, D. Benitez-Ribas, V. Ortiz-Maldonado, J. Cid, J. Tabera, J. M. Canals, M. Lozano, T. Baumann, A. Vilarrodona, E. Trias, E. Campo, P. Menendez, Á. Urbano-Ispizua, J. Yagüe, P. Pérez-Galán, et al., *Mol. Ther.–Methods Clin. Dev.* **2019**, *12*, 134.
[76] J. E. Dahlman, C. Barnes, O. F. Khan, A. Thiriot, S. Jhunjunwala, T. E. Shaw, Y. Xing, H. B. Sager, G. Sahay, L. Speciner, A. Bader, R. L. Bogorad, H. Yin, T. Racie, Y. Dong, S. Jiang, D. Seedorf, A. Dave, K. Singh Sandhu, M. J. Webber, T. Novobrantseva, V. M. Ruda, A. K. R. Lytton-Jean, C. G. Levins, B. Kalish, D. K. Mudge, M. Perez, L. Abezgauz, P. Dutta, L. Smith, et al., *Nat. Nanotechnol.* **2014**, *9*, 648.
[77] T. Wei, Q. Cheng, Y.-L. Min, E. N. Olson, D. J. Siegwart, *Nat. Commun.* **2020**, *11*, 3232.
[78] R. H. Kutner, X.-Y. Zhang, J. Reiser, *Nat. Protoc.* **2009**, *4*, 495.
[79] D. Mai, O. Johnson, J. Reff, T.-J. Fan, J. Scholler, N. C. Sheppard, C. H. June, *Proc. Natl. Acad. Sci. U. S. A.* **2023**, *120*, 2218632120.